№1, 2023

ISSN 2706-977X

SAGINOV TECHNICAL UNIVERSITY

MATERIAL AND MECHANICAL ENGINEERING TECHNOLOGY

Content

DOI 10.52209/2706-977X_2023_1_3 IRSTI 53.49.13 UDC 621.891

Influence of Dynamic Viscosity of a Lubricant Material on the Parameters of Adhesion Bond in the Systems of Materials "12KH2H4 - STEEL 45", "45KHN2MFA - Steel 45" when Boring and Borocement Steel 45

Kubich V.I.[1], Cherneta O.G.[2], Yurov V.M.[3*]
[1]National University "Zaporizhzhya polytechnic", Zaporizhia, Ukraine
[2]Dniprovsk State technical university, Kamenskoye, Ukraine
[3]Karaganda Buketov University, Karaganda, Kazakhstan
*corresponding author

Abstract. In this work, the regularities of the change in the shear strength of the adhesive bond τ_0 and the piezoelectric coefficient β in the metal systems "12Kh2N4 (45KhN2MFA) - steel 45 + B", "12Kh2N4 (45KhN2MFA) - steel 45 + VS" were obtained during physical modeling of the shear of surfaces of small-sized samples and changes in dynamic viscosity environment of their interaction with the use of additional equipment of the SMTs-2 friction machine. It has been established that borating and boron carburizing of the surface of steel 45 leads to the absence of adhesion to the surfaces of steels 12Kh2N4 and 45KhN2MFA in certain ranges of normal pressures, at which $\tau_0 > 0$ and the dynamic viscosity of liquid and grease. It was found that the parameter τ_0 when lubricating surfaces is determined to a greater extent for the system "12X2H4 - steel 45", and partially for borating steel 45 and low values of dynamic viscosity μ = 0.027 Pa•s. With an increase in the dynamic viscosity of the liquid phase of the lubricant in the "12X2H4 - steel 45" system, there is a tendency to an increase in the value of τ0. It was found that the absence of modification of steel 45 with boron and boron carbide predetermines the independence of the piezoelectric coefficient from the viscosity of the liquid lubricant and the shear rate. Boring and boron carburizing steel 45 predetermines an increase in the piezoelectric coefficient by an average of 1.6 times with an increase in dynamic viscosity from 0.027 Pa•s to 0.19 Pa•s at a shear rate of 10.16±0.8. At shear rate = 5.08±0.6 mm/s, the piezoelectric coefficient is relatively constant in the systems under study. With the transition to contact through a grease lubricant, there is an ambiguous manifestation of the rate of change of the piezoelectric coefficient.

Key words: piezo coefficient, dynamic viscosity, lubricant, shear rate, tangential strength

Introduction

Forecasting the resource of mechanisms of mechanical engineering objects presupposes the presence of certain initial data. In this case, the main quantity is the wear rate of the surfaces of materials, which is determined both experimentally and theoretically. So, for example, when calculating the service life of a gear pair, it is necessary to know not only the geometric parameters of the engagement, but also the parameters of the adhesion properties and fatigue of the contacting surfaces. This is especially important when measures are proposed to modify the working surfaces to improve the physical and mechanical properties of metals. The existing structural alloy steels 12Kh2H4, 45KhH2MFA, high-quality carbon steel 45 are widely used for the manufacture of a wide range of mechanical engineering parts, including gears, gear shafts of gear drives for various purposes. Undoubtedly, the presence of numerical values of the parameters of the adhesion properties of the listed jointly working metals will determine the accuracy of the calculations performed, and the possible surface modification of one of them will expand the information on the nature of its influence on the manifestation of these parameters. Based on the above, the establishment of regularities in the manifestation of the parameters of adhesion properties in systems of structural metals seems to be an urgent scientific and fundamental task considered in tribology.

1. Review of previous publications, setting the goal of the work

The technology of surface modification of steel 45 by borating and boron cementation is proposed, which predetermines the change in both the phase composition of the surface structures and their hardness [1-3].

In [4], the regularities of the change in the shear strength of the adhesive bond τ0 and the piezoelectric coefficient β in the metal systems "steel 45 - 40X", "steel 45 + B - 40X", "steel 45 + BC - 40X" were obtained during physical modeling of the shear between small samples in the environment of lubricants I-20A, Wolf 10W-40, TAD-17i, Litol-24 with distinctive dynamic viscosities using additional equipment of the SMTs-2 friction machine. At the same time, the features of the manifestation of the parameters of the adhesion bond depending on the shear rate have been established. The results obtained are typical for systems of materials in which alloyed structural steel 40X is a constant element. This steel has one alloying element chromium, which predetermines the amount of surface energy, due to a greater extent to the chemical element - iron.

Steels 12Kh2N4, 45KhN2MFA can be alternative steel 40Kh structural metals, for example, as discussed above, for the manufacture of gears. Moreover, they have a different content of chemical elements, and, accordingly, surface energy (surface tension [5, 6]), which will affect the formation of adhesive interaction in contact with steel 45 when it is modified with boron and boron carbide. Moreover, the hardness of steels 12Kh2N4, 45KhN2MFA is less than steel 40Kh. From this, it is evident that it is necessary to perform not only an assessment of the manifestation of adhesion parameters in systems of metals with steels 12Kh2N4, 45KhN2MFA, but also to establish their change depending on the decrease in the hardness of one of the elements of the friction pair, in this case it is a direct pair.

The aim of the work is to establish the regularities of changes in the parameters of the adhesive bond in the systems of materials "steel 45 – 45KhN2MFA", "steel 45 + B - 45KhH2MFA", "steel 45 + VS - 45KhH2MFA", "steel 45 - 12Kh2H4", "steel 45 + B - 12Kh2H4 "," steel 45 + BC - 12Kh2H4 "in the physical modeling of the shift between small-sized samples in the environment of lubricants with distinctive dynamic viscosities using additional equipment of the SMTs-2 friction machine.

Based on the above, this work seems to be a continuation of the complex of studies begun in [3, 4, 7].

2. Research methodology

The parameters of the adhesive bond were evaluated using an SMTs-2 friction machine with additional equipment in accordance with the procedure described in [7]. In this case, movable samples - disks were made of steels 12Kh2N4, 45KhN2MFA, and fixed pads in the form of triangular-shaped segments of steel 45 with surface modification with boron and boron carbide, i.e. the same samples were used as in [4]. To estimate the pressure in the contact zone and the tangential shear strength, we used the average values of the contour areas, which were determined from the indentations. The modeling of the manifestation of the properties of the lubricating medium was carried out using the same lubricants as in [4]. The following lubricants were applied to the surface of the samples:

- industrial oil I-20A (GOST 20799-88), dynamic viscosity at 40 ºC μ = 0.027 Pa•s;
- transmission oil TAD-17i (GOST 23652-79), dynamic viscosity at 50 ºC μ = 0.106 Pa•s;
- semi-synthetic motor oil Wolf 10W-40 API SL/SF, dynamic viscosity at 40 ºC μ = 0.19 Pa•s;
- Litol-24 grease (GOST 21150-2017), dynamic viscosity at 50 ºC μ = 8 Pa•s.

This choice of lubricants determined, firstly, different values of the dynamic viscosity for the liquid state of aggregation of the lubricating medium, and secondly, the presence of a consistent medium. This makes it possible to take into account the possible contact interaction of the surfaces of the teeth of gears of various gears, for example, in mechanical drives of machine tools, transmission units for cars and tractors, gearboxes of hand-held power tools.

To assess the parameters of adhesion without lubricant, the surfaces were thoroughly degreased with gasoline "Kalosha".

3. Research results and their discussion

As a result of processing the tribograms of the shear surfaces of a stepwise loaded contact in the considered systems of materials, statistical data were obtained, which are summarized in Tables 1, 2.

Table 1. Parameters of approximation of experimental data for the system of materials "45KhN2MFA - steel 45 (+ B, + VS)" in the environment of lubricants

Parameter	Steel 45				Steel 45+B				Steel 45+BC			
Lubricant	I-20	TAD-17и	Wolf 10W40	Lithol -24	I-20	TAD-17и	Wolf 10W40	Lithol -24	I-20	TAD-17и	Wolf 10W40	Lithol -24
Piezo coefficient β	$\tau = 0{,}11p + 3{,}58$ -				$\tau = 0{,}05p + 5{,}6$ $\tau = 0{,}14p - 0{,}24$				$\tau = 0{,}24p - 18{,}9$ $\tau = 0{,}38p - 33{,}3$			
	0,12	0,13	0,12	0,12	0,15	0,13	0,17	0,12	0,11	0,1	0,14	0,15
	-	-	-	-	0,24	0,21	0,21	0,17	0,14	0,14	0,16	0,13
Tangential strength τ_0, MPa	2,02	>0 at p≈23 MPa	>0 at p≈2 MPa	>0 at p≈23 MPa	>0 af p≈30 MPa	>0 at p≈26 MPa	>0 at p≈58 MPa	>0 at p≈38 MPa	>0 at p≈23 MPa	>0 at p≈18 MPa	>0 at p≈52 MPa	>0 at p≈23 MPa
	-	-	-	-	>0 at p≈40 MPa	>0 at p≈48 MPa	>0 at p≈46 MPa	>0 at p≈40 MPa	>0 at p≈24 MPa	>0 at p≈18 MPa	>0 at p≈56 MPa	>0 at p≈88 MPa

Note. 1. The upper row of values at a shear rate υ_1 = 10.16 ± 0.8 mm/s, the lower one at υ_2 = 5.08 ± 0.6 mm/s.

2. The equation of the form is given for a system without lubricant.

Analysis of the data obtained indicates the following.

First, the parameter τ0 is determined only:

- in the absence of lubricant for the system "45KhN2MFA - steel 45". In this case, exclusively boronization of the surface of steel 45 leads to a slight increase in the value of τ0 from 3.58 MPa to 5.6 MPa;

- when lubricating surfaces to a greater extent for the system "12Kh2H4 - steel 45" in the absence of surface modification of steel 45, as well as when it is borated and low values of dynamic viscosity μ = 0.027 Pa•s. In this case, with an increase in the dynamic viscosity of the liquid phase of the interaction lubricant, a tendency to an increase in the value of τ_0 is observed. To a lesser extent, this parameter manifested itself for the system "45KhN2MFA - steel 45" again with dynamic viscosity μ = 0.027 Pa•s, but without modification of steel 45.

Table 2. Parameters of approximation of experimental data for the system of materials "12Kh2H4 - steel 45 (+ B, + BC)" in the environment of lubricants

Parameter	Steel 45				Steel 45+B				Steel 45+BC			
Lubricant	I-20	TAD-17*и*	Wolf 10W40	Lithol -24	I-20	TAD-17*и*	Wolf 10W40	Lithol -24	I-20	TAD-17*и*	Wolf 10W40	Lithol -24
Piezo coefficient *β*	$\tau = 0,36p - 13,44$				$\tau = 0,2p - 10,5$				$\tau = 0,33p - 32,3$			
	-				$\tau = 0,2p - 5,56$				$\tau = 0,37p - 33,8$			
	0,1	0,11	0,1	0,15	0,11	0,18	0,17	0,1	0,18	0,16	0,18	0,13
	-	-	-	-	0,15	0,15	0,15	0,14	0,11	0,14	0,14	0,12
Tangential strength τ_0, MPa	8.3	4,8	10,7	>0 at *p*≈24 MPa	1,0	>0 at *p*≈30 MPa	>0 at *p*≈54 MPa	1,0	>0 at *p*≈42 MPa	>0 at *p*≈44 MPa	>0 at *p*≈60 MPa	>0 at *p*≈5 MPa
	-	-	-	-	1,21	>0 at *p*≈17 MPa	0,5	>0 at *p*≈17 MPa	0,1	>0 at *p*≈62 MPa	>0 at *p*≈58 MPa	>0 at *p*≈38 MPa

Note. 1. The upper row of values at a shear rate υ_1 = 10.16 ± 0.8 mm/s, the lower one at υ_2 = 5.08 ± 0.6 mm/s.

On the whole, the results obtained confirm the thesis given in [5] on the structural sensitivity of the adhesive parameters. The manifestation of the adhesive interaction parameter τ0 in the absence of lubrication can be explained by the ratio of the hardness of the interacting surfaces. According to the research conditions, H12Kh2H4 <H45KhH2MFA <H45, and H45 <H45 + B <H45 + BC. From which it follows that in each of the contact options, the parameter τ_0 is extrapolated back after the manifestation of plastic, elastic-plastic and elastic deformation of the microprofiles of metal surfaces. Such interaction can be estimated in accordance with the relaxation theory of adhesion, which considers deformation processes, the appearance of internal stresses in the thinnest surface layers and their subsequent relaxation [8]. In this case, the deformable metal layers have different thicknesses with one interface. When the load is removed during elastic deformation, the dimensions are restored, i.e. there is a sufficiently large supply of internal mechanical energy in the near-surface layers. From which it follows that such an energy reserve is capable of forming, among other things, the action of surface forces of adhesive interaction. While the supply of such energy can be critically maximum only up to a certain value from the point of view of a possible increase in the surface energy of one of the components of the system. This is exactly what happened when modifying steel 45 with boron carbide, i.e. it is possible to change the mechanism of adhesive interaction by the nature of its appearance.

The manifestation of the parameter τ_0 of adhesive interaction in a lubricating medium can be explained by a large adsorption decrease in surface strength (Rebinder effect) for a less solid component of the system of materials, which predetermines the formation of the manifested large adhesion forces with a harder surface. Those. the less solid surface of the component of the metal systems under study seems to be more susceptible to penetration of the less viscous liquid phase of the lubricant, which manifested itself for the system "12Kh2H4 - steel 45". Based on the above, the considered interaction can be estimated in accordance with the theory of weak boundary layers [8]. In accordance with this theory, "weak" boundary layers with physicochemical properties that differ from those of the underlying layers are formed in the contact zone. In this case, it is the "weak" layers that determine the strength of the adhesive bond. In this case, the deformable metal layers have different thicknesses, but already with two interfaces. The first interface is formed by the elements "body (rotating disk, material 12Kh2H4, 45KhH2MFA) - a near-surface layer of a lubricant with bulk properties". The second surface is "a near-surface layer of a lubricant with bulk properties - a counterbody (fixed block, material steel 45"). From which it follows that the shear fracture mechanism can be not only cohesive [8], ie. within the adsorbed and deformed molecules of the lubricant (transition regions), but also mixed, taking into account the destruction of bonds along the interfaces. The latter is explained by the characteristics of the microprofiles of the contacting surfaces, which causes uneven deformation of the lubricant molecules distributed between them.

Second, borating and boron carburizing of the surface of steel 45 leads to the absence of adhesion to the surfaces of steels 12Kh2N4 and 45KhN2MFA in certain ranges of normal pressures, at which $\tau_0 > 0$. This range is determined by the upper limit of the mechanical pressure p. In general, the following holds:

- a larger range of pressures is typical for the system "12Kh2H4 - steel 45", which, for example, at a shear rate of $\upsilon_1 = 10.16 \pm 0.8$ mm/s for liquid lubricant is from 0 to 42 MPa when borated steel 45, and from 0 to 48 MPa with its boron carburizing. For grease, this range is much smaller - from 0 to 17 MPa for borating, and from 0 to 5 MPa for boron carburizing. At the same time, a twofold decrease in the shear rate leads to a decrease in the average range in a liquid medium by 2.5 times during boriding, and an increase in the range by 1.25 times for a liquid lubricant during boron cementation;

- a smaller range of pressures is typical for the system "45KhN2MFA - steel 45", which, for example, at a shear rate of $\upsilon_1 = 10.16 \pm 0.8$ mm/s for a liquid lubricant is from 0 to 38 MPa when borated steel 45, and from 0 to 31 MPa with its boron carburizing. However, for grease, this range appeared from 0 to 38 MPa for borating, and from 0 to 23 MPa for boron carburizing. At the same time, a twofold decrease in the shear rate leads to an insignificant increase in the average range in a liquid medium during boriding, and its equality for a liquid lubricant during boron cementation. For grease, the range was preserved within the same boundaries during borating as in a liquid medium, and its increase by 3.8 times during boron cementation. For a more detailed and visual assessment of the dependence of the upper pressure limit on the change in the dynamic viscosity of the liquid lubricant in accordance with the data of table 1, 2, graphical dependencies are built, Fig. 12.

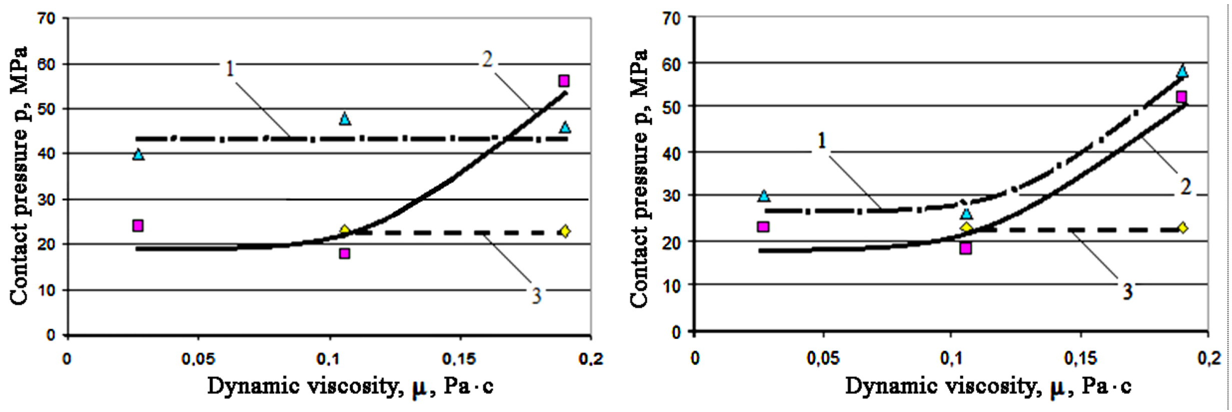

a) at $\upsilon_2 = 5.08 \pm 0.6$ mm/s; b) at $\upsilon_1 = 10.16 \pm 0.8$ mm/s; 1) steel 45 when borated; 2) with boron carburizing steel 45; 3) steel 45 without modification

Fig. 1. - Influence of dynamic viscosity on the manifestation of adhesion in the system of materials "45KhN2MFA - steel 45" by pressure in contact

From Figure 1 it follows that in the material system "45KhN2MFA - steel 45", the change in the dynamic viscosity of the liquid lubricant, starting from 0.11-0.12 Pa • s, predetermines an increase in the pressure of the beginning of the manifestation of adhesion forces during boron cementation of steel 45 and the shear rate of 5.08 ± 0.6 mm/s. The same takes place when it is borated and boron-cemented, but at a shear rate of 10.16 ± 0.8 mm/s. At the same time, the intensity of its growth remains unchanged. The viscosity in the range from 0.01 to 0.11 Pa•s does not affect the change in the beginning of the manifestation of adhesion between the surfaces during borating and boron-carburizing steel 45. The viscosity also does not affect the beginning of the manifestation of adhesion between the surfaces of the systems under study, even in the absence of modification, steel 45.

From Figure 2 it follows that in the system of materials "12Kh2H4 - steel 45" only at a shear rate of 10.16 ± 0.8 mm/s, a change in viscosity causes a linear increase in the pressure of the beginning of the manifestation of adhesion forces during boron carburizing of steel 45 in the entire modeled range. The same effect of viscosity occurs during borating steel 45, but in the range from 0.11 to 0.2 Pa s, however, the increase in values occurs with greater intensity.

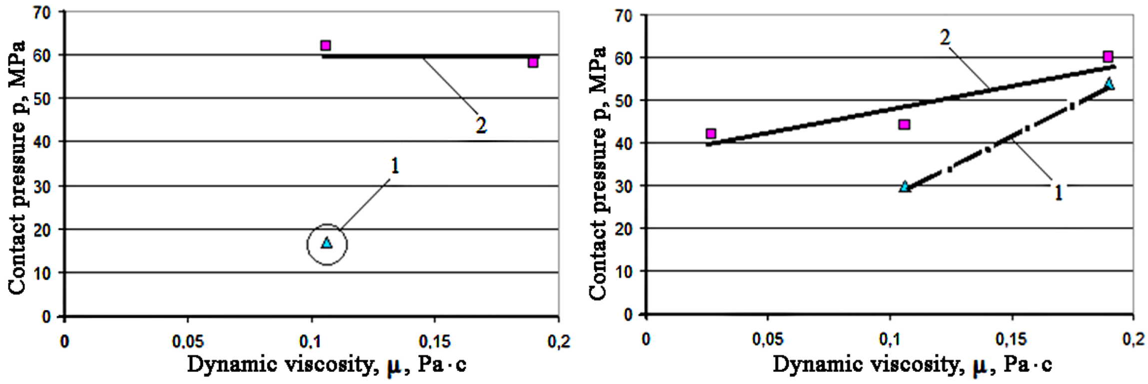

a) at υ_2 = 5.08 ± 0.6 mm/s; b) at υ_1 = 10.16 ± 0.8 mm/s; 1) steel 45 when borated; 2) with boron carburizing steel 45

Fig.2. - Influence of dynamic on the manifestation of adhesion in the system of materials "12Kh2H4 - steel 45" by pressure in contact

The obtained and described results on the parameter τ_0 generally indicate the ambiguity and peculiarity of the manifestation of adhesion between the studied surfaces of steels, activated for interaction by the supply of external mechanical energy of high mechanical pressures, excess surface energies due to the introduction of additional chemical elements during the modification of steel 45 and components of the used lubricating media. ... At the same time, it should be noted the effect of a short-term structural change in liquid lubricants on the contour contact areas during their compression, since the design pressures are sufficiently high. The pressures in the zone of frictional interaction ranged from 80 MPa to 260 MPa. Due to the complexity and versatility of the components of these processes and the limited information on their course, this issue is not discussed in the work and remains open.

Thirdly, the parameter β has a simpler and rather informative calculated manifestation. For a more visual assessment, graphical approximations of the trends in the change in the piezoelectric coefficient in the considered systems of materials when modeling the shear rate in the range of dynamic viscosity of liquid lubricants are shown in Fig. 3, 4.

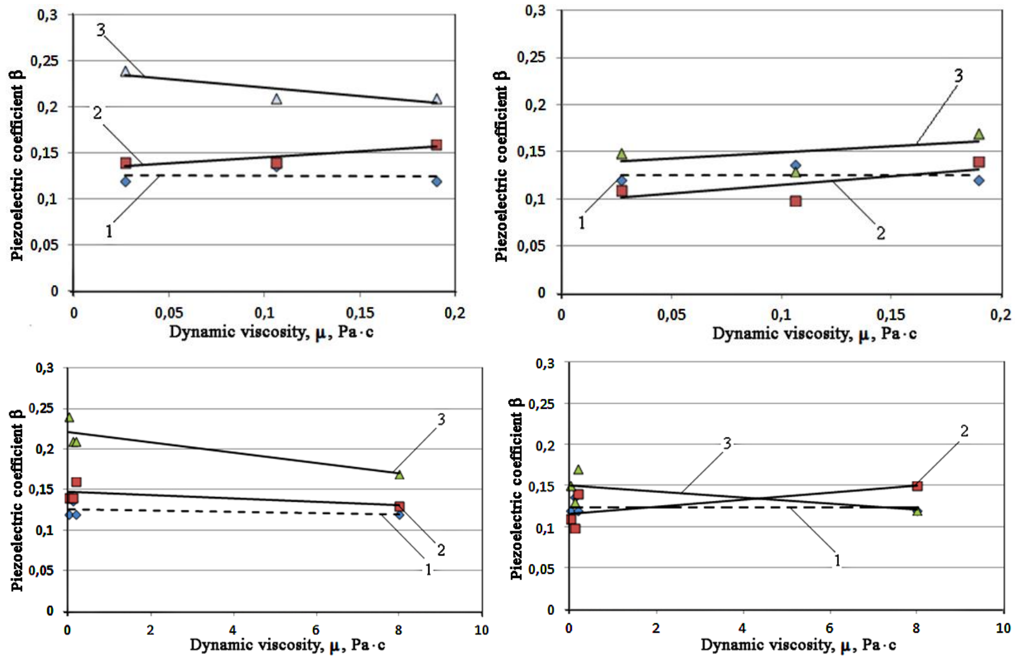

a, b) at = 5.08 ± 0.6 mm/s; b, d) at = 10.16 ± 0.8 mm/s; 1) steel 45 is not modified; 2) "steel 45 + BC"; 3) "steel 45 + B"

Fig. 3. - Influence of dynamic viscosity in the range of liquid (a, b) lubricant and taking into account the range of consistent state (c, d) on the change in the piezoelectric coefficient of adhesive bond in the material system "45KhN2MFA - steel 45"

The analysis of the presented dependencies in Fig. 3,4 indicates the following.

First, the absence of modification of steel 45 with boron and boron carbide predetermines the independence of the piezoelectric coefficient from the viscosity of the liquid lubricant and the shear rate. In the simulated ranges of viscosity and shear rate, the increment of the piezoelectric coefficient values is zero. The exception is the system "12Kh2H2 - steel 45". For this system of metals with the transition to a grease lubricant, the rate of increase in the piezoelectric coefficient is 0.0064 $(Pa\ s)^{-1}$. At the same time, the average statistical values of the piezoelectric coefficient are: for the system "12Kh2H2 - steel 45" in the viscosity range from 0.001 Pa • s to 0.2 Pa•s $\beta = 0.1 \pm 0.003$, for the system "45KhN2MFA - steel 45" $\beta = 0,12 \pm 0.003$. From which it seems obvious that the intensity of the increase in the strength of the adhesive bond in the system "45KhN2MFA - steel 45" is 1.2 times higher.

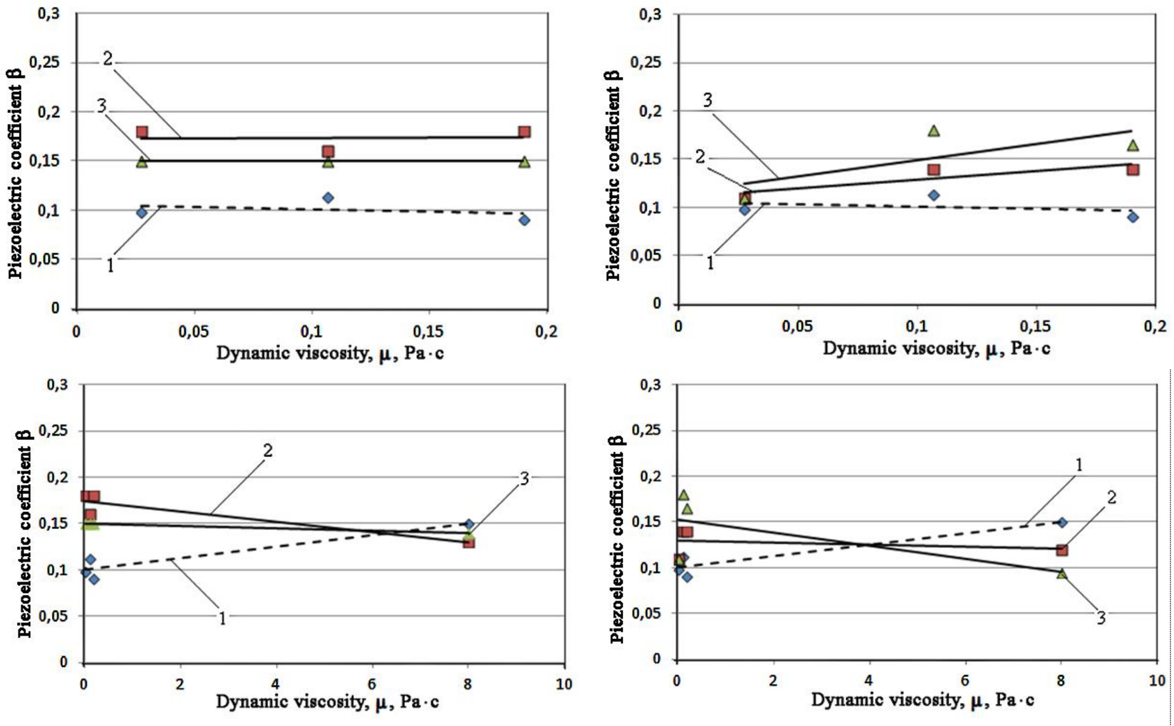

a, b) at = 5.08 ± 0.6 mm/s; b, d) at = 10.16 ± 0.8 mm/s; 1) steel 45 is not modified; 2) "steel 45 + BC"; 3) "steel 45 + B"

Fig. 4. - Influence of dynamic viscosity in the range of liquid (a, b) lubricant and taking into account the range of the consistent state (c, d) on the change in the piezoelectric coefficient of adhesive bond in the material system "12Kh2H2 - steel 45"

Secondly, boriding and boron carburizing steel 45 predetermines an increase in the piezoelectric coefficient by an average of 1.6 times in the range of viscosity of a liquid lubricant and a shear rate of 10.16 ± 0.8. At shear rate = 5.08 ± 0.6 mm/s, the piezoelectric coefficient is relatively constant in the systems under study. With the transition to contact through a grease lubricant, there is an ambiguous manifestation of the rate of change of the piezoelectric coefficient. For the system "12Kh2H2 - steel 45 + B (BC)" with a shift of 5.08 ± 0.6 mm/s, the rate of decrease of the piezoelectric coefficient is 0.005 $(Pa•c)^{-1}$. From which it follows that modification with boron and boron carbide predetermines a less intense increase in the strength of the adhesive bond of the investigated metal surfaces.

Conclusion

The results obtained in the work revealed the features of the manifestation of the adhesive bond parameters in the investigated metal systems when simulating changes in dynamic viscosity in the range from 0.027 Pa•s to 8 Pa•s.

The constructed graphic patterns and the parameters of their mathematical approximation made it possible to determine the direction of the processes of adhesive interaction of the surface of 45 steel modified with boron and boron carbide with steels 12Kh2N2, 45KhN2MFA through lubricating formations compacted by contact pressure with distinctive gradients of dynamic viscosity.

It has been established that the borating and boron cementation of steel 45 predetermines the expansion of the range of working normal pressures in lubricating media, excluding the manifestation of the adhesive friction component, and in contact with steel 45KhN2MFA upwards.

The data obtained can be used, firstly, as reference values of the adhesive bond parameters to substantiate the possibilities of increasing the reliability of the operation of friction pairs during shear, and secondly, when calculating the service life of a gear pair, in which the gears will be made from the studied systems of materials.

The direction of further research is proposed to consider the study of the nature of the relationship between the manifestation of the established parameters τ_0 and β and the surface energies of the contacting surfaces of the metal systems under consideration.

References

[1] Cherneta O.G., Kubich V.I., Voloshchuk R.G, Averyanov V.S., Shmatko D.Z. Strengthening of the Restored Surface Layer of Steel Parts 45 by Laser Boring // International Journal of Engineering & Technology (UAE). Science Publishing Corporation, RAK Free Trade Zone, 2018, Vol 7, No 4.3. - P.71-75.

[2] Sitkevich M.V., Pishchov M.N., Belsky S.E. The influence of complex boride hardening on the structure and properties of the surface layers of steels for the manufacture of gear parts for skidding forest machines // Casting and metallurgy, 2008, No. 4(49). - P. 140-146.

[3] Cherneta O.G., Kubich V.I., Shcherbina M.A., Averyanov V.S., Shmatko D.Z. Research of steel 45 strugging influence on the parameters of adhesion communication with chrome, chrome-nickel steel // Mathematical modeling, 2019, No. 2 (41). - P. 150-158.

[4] Kubich V.I., Cherneta O.G., Yurov V.M. Influence of borination, borocement of steel 45 and viscosity of a lubricant on the parameters of adhesion bond in the steel 45-40X system // Eurasian Physical Technical Journal, 2021, Vol 18, No 2(36). - P.67-75

[5] Semenov V.I., Shuster L.Sh., Chertovskikh S.V., Raab G.I. Influence of the complex parameter of plastic frictional contact and material structure on the strength of adhesive bonds // Friction and Wear, Vol. 26, No. 1.,2005. - P. 74-79.

[6] Yurov V.M., Eremin E.N., Guchenko S.A. Application of high entropy coatings simultaneous in one cycle spraying three cathodes // Bulletin of KarSU. Physics, No. 1(97), 2020. – P. 7-17.

[7] Kubich V.I., Cherneta O.G., Yurov V.M. Potential difference of metal machine parts methodology for determining the parameters of adhesional properties of materials on the SMC-2 friction machine // Eurasian Physical Technical Journal, 2019, Vol.16, No. 2(32). – P. 78-82.

[8] Bogdanova Yu.G. Adhesion and its role in ensuring the strength of polymer composites. - M.: MGU, 2010. – 132 p.

Information of the authors

Kubich Vadim Ivanovich, Candidate of Technical Sciences, Associate Professor, National University "Zaporozhye Polytechnic"
e-mail: schmirung@gmail.com

Cherneta Oleg Georgievich, Candidate of Technical Sciences, Associate Professor, Dniprovsk State Technical University
e-mail: ocherneta@gmail.com

Y**urov Viktor Mikhailovich,** Candidate of Physical and Mathematical Sciences, Associate Professor, Karaganda Buketov University
e-mail: exciton@list.ru

DOI 10.52209/2706-977X_2023_1_10 IRSTI 53.45.15 UDC 669.245.018.44

Anisotropy of the Surface Energy of Steel and Nickel Alloys in Aviation

Yurov V.M.[1], Goncharenko V.I.[2,3], Portnov V.S.[1], Sha Mingun[4], Oleshko V.S.[2], Rakhimova Zh.B.[1], Rakhimov M.A.[1], Rakhimova G.M.[1*], Maussymbayeva A.D.[1]

[1]Abylkas Saginov Karaganda Technical University, Karaganda, Kazakhstan

[2] Moscow Aviation Institute (National Research University), Moscow, Russia

[3]Institute for Management Problems. V.A. Trapeznikova, RAS, Moscow, Russia,

[4]Northwestern Polytechnic University, Yangtze River Delta Research Institute of Northwestern Polytechnic University, Taicang, China

*corresponding author

Abstract. The article presents the values of the thickness of the surface layer and the surface energy of steel and nickel parts of the aircraft industry. The thickness of the surface layer for the face (100) is about 1.7 nm, which coincides with the thickness of the surface layer of iron - R(I)=M/ρ = 1.7 nm, since iron in these steels is more than 70%. The R(I) layer contains ≈ 6 iron monolayers. In the [111] plane, the lowest value of the surface energy (~1060 mJ/m^2) is observed. The average thickness of the surface layer of nickel alloys is R(I) ≈ 2 nm, and the number of monolayers is ≈ 6. This value coincides with the number of iron monolayers. The average value of the surface energy of nickel alloys is greater than that of iron-based alloys.

The article shows that the hardness of high-entropy (HEA) coatings and metallic glasses (ML) is approximately the same, but almost 2 times higher than the hardness of steel and nickel coatings. For HEAs and MS coatings, the thickness of the surface layer is also approximately the same. In our opinion, there are many similarities between high-entropy alloys and metallic glasses.

The friction of steel and nickel coatings lies at the level of 0.4-0.6. For metallic glasses, the coefficient of friction is higher than 0.2 or more. For HEAs, the coefficient of friction is much less than 0.1.

Keywords: nanostructures, surface layer thickness, surface energy, anisotropy, high-entropy coatings, friction, metal, alloy, hardness.

Introduction

This work is a continuation of works [1-3], where for the first time a model of the surface layer of perfect single crystals was constructed and the role of surface energy in physical processes occurring in the nanoscale region was elucidated. Russia, Kazakhstan and China are present in all stages of production, both military and civil aviation and space. This forces her to engage in the development and production of aircraft and spacecraft of various types. Today, in terms of the total production of aircraft, Russia ranks third after the USA and France, but in terms of the production of components for aviation, it is only in seventh place in the world [4].

The constant improvement of aircraft designs required a continuous increase in strength and specific strength (the ratio of strength to material density) while maintaining all the advantages of steels. If in aviation before 1941 the first of these parameters ranged from 800 to 1000 MPa, now it is from 1300 to 2000. However, the complexity of the problem lies not so much in achieving such indicators, but in ensuring the operability of aircraft structures made of appropriate materials. The fact is that an increase in the strength of steels leads to a decrease in their ductility, toughness, crack resistance, etc. In this regard, the developers of their new varieties are constantly searching for compromises between increasing strength and ensuring reliability. Currently, three groups of high-strength steels are most often used in aviation technology: structural medium-alloyed; corrosion resistant; used for the manufacture of parts operating in difficult conditions with increased friction and subjected to chemical-thermal treatment [5].

Many publications appeared on the problems of aircraft construction and their materials. It is possible to list only dissertations completed in the last 2–3 years, where an bibliography is presented [6–12].

1. Steel alloys in aviation

In aircraft construction, steel alloys still remain the basis of structural materials that can be divided into three groups: high-strength steels, medium-alloyed steels, and corrosion-resistant steels that operate under high friction conditions and are subjected to thermal and chemical attack [13-17]. Compared to conventional steels with a strength of up to 1400 MPa, steels with a strength of up to 2500 MPa are needed, while parts made of these steels must be wear-resistant, that is, resistant to corrosion, mechanical and heat treatments. This is achieved by reducing surface and subsurface defects. Thus, knowledge and control of the surface of materials and parts in the aircraft industry is an urgent problem. Steel VKS-8 (1800-2000 MPa) and steel VKS-9 (1950-2100 MPa) are used in the manufacture of large-sized aircraft parts, for example, landing gear. They successfully replace titanium alloys, which are much more expensive. Not so long ago, they began to melt the maraging steel VKS-180-ID, which has a strength of 1450–2500 MPa and unique mechanical and technological characteristics [15]. Due to the low content of carbon and nitrogen, they are characterized by high ductility and toughness, which leads to the production of complex-shaped parts (MiG-31 and MiG-29 parts). Steel VKS-9 and VKS-180-ID are shown in fig. 1 and fig. 2. VNS-2 steel, which is resistant to corrosion, is used for plating aircraft of various classes. For the production of such parts as bars, forgings, steels EP817, VNS-25, VNS-41, VNS=49, VNS-50, CH-2A and others are used. The chemical composition of some of the steels listed above is shown in Table 1.

The most loaded unit of aircraft engines is the blade of the first stage of the turbine, which, due to the high thermal stress and corrosion of the external environment, has a short service life of the aircraft engine as a whole [10, 11, 18, 19].

Fig. 1. - Aircraft landing gear from steel VKS-9

Fig. 2. - Martensite-aging steel VKS-180-ID

Table 1. Chemical composition of aviation alloys

Alloy	Fe	C	S	P	Mn	Cr	Si	Ni	Cu	Ti	Mo	Co
VNS-2-Sh	77,7-74,9	< 0,08	0,018	0,02	1,0	14-15	0,7	4,7-5,5	1,75-2,5	0,15-0,3	-	-
VNS-25	76,5-73,2	0,03	0,01	0,01	0,25	11,5-12,5	0,25	9,0-10,3	0,2 Al 0,003 B	0,15-0,25	0,5-0,6	0,05Ca 0,1Zr
EP817	73,95-73,22	0,05-0,08	-	-	1,0	13,5-14,5	0,7	5,6-6,2	1,8-2,2	0,03-0,1	1,3-1,7	0,3 Nb

A major role here is in the creation of new alloys, which are subject to the following requirements:

- the alloy should be distinguished by a high index of long-term strength and high creep at high-temperature operation;
- the alloy must be characterized by a low atomic diffusion coefficient and a stable structure;
- the alloy should be characterized by high fatigue strength and low sensitivity to residual stresses;
- the alloy should have a lower specific gravity.

According to the international classification, several single-crystal generations of heat-resistant nickel alloys (HNS) have been created for the manufacture of turbine blades of a gas turbine engine (GTE) [20]. The first generation includes alloys of elements that are necessary for alloying: Al, Ti, Cr, Mo, Co, W, Ta, Nb. The second and third generations contain, in addition to the first generation, also rhenium in the amount of 2-4% and 5-6%, respectively. The fourth and fifth generations contain the element ruthenium in addition to rhenium. In ZHNS alloys, various chemical elements are contained in various proportions (Table 2).

Table 2. Chemical composition and density of single-crystal heat-resistant nickel alloys (ZhNS) [21]

Alloy	Content, % (by mass), alloying elements											Density g/cm^3
	Cr	Ti	Mo	W	Re	Ta	Al	Co	Nb	Hf	etc.	
First generation												
ЖС30М	-	1,8	0,6	11,7	-	-	5,1	7,5	1,1	0,1	-	8,635
ЖС40	6,1	-	4,0	6,9	-	7,0	5,6	5,0	-	-	-	8,84
PWA-1480	10,0	1,5	-	4,0	-	12,0	5,0	5,0	-	-	-	8,70
CMSX-2	8,0	1,0	0,6	8,0	-	6,0	5,6	5,0	-	-	-	8,56
CMSX-3	8,0	1,0	0,6	8,0	-	6,0	5,6	4,6	-	0,1	-	8,60
SSR99	8,0	2,2	-	10,0	-	3,0	5,5	5,0	-	-	-	8,56
RR2000	10,0	4,0	3,0	-	-	-	5,5	15,0	-	-	1,0V	7,87
MC2	8,0	1,5	2,0	8,0	-	6,0	5,0	5,0	-	-	-	8,63
AM1	7,8	1,1	2,0	5,7	-	7,9	5,2	6,5	-	-	-	8,59
AM3	8,0	2,0	2,25	5,0	-	3,5	6,0	5,5	-	-	-	8,25
DD3	9,5	2,0	4,0	5,5	-	-	5,8	5,0	-	-	-	8,20

Second generation											
ЖС36	4,0	1,1	1,6	11,7	2,0	-	5,8	7,0	1,1	-	-	8,724
CMSX-4	6,5	1,0	0,6	6,0	3,0	6,5	5,6	9,0	-	0,1	-	8,70
Rene N5	-	-	2,0	5,0	3,0	7,0	6,2	8,0	-	0,2	0,05C	8,63
SCI80	5,0	1,0	2,0	5,0	3,0	8,5	5,2	10,0	-	0,1	-	8,84
SMP14	4,8	-	1,0	7,6	3,9	7,2	5,4	8,1	1,4	-	-	-
PWA-1484	5,0	-	2,0	6,0	3,0	8,7	5,6	10,0	-	0,1	-	8,95
TMS-71	6,0	-	6,4	-	2,5	8,4	5,7	6,0	-	-	-	-
TMS-82	4,9	0,5	1,9	8,7	2,4	6,0	5,3	7,8	-	0,1	-	8,90
DD6	4,3	-	2,0	8,0	2,0	7,5	5,6	9,0	0,5	0,1	-	8,83
CMSX-8	5,4	0,7	0,6	8,0	1,5	8,0	5,7	10,0	-	0,1	-	8,85
Third generation												
Rene N6	4,2	-	1,4	6,0	5,4	7,2	5,75	12,5	-	0,15	0,05C 0,004B 0,01Y	8,97
CMSX-10	2,0	0,2	0,4	5,0	6,0	8,0	5,7	3,0	0,1	0,03	-	9,05
CMSX-10M	2,0	0,24	0,4	5,4	6,5	8,2	5,78	-	0,08	0,03	-	9,02
TMS-75	3,0	-	2,0	6,0	5,0	6,0	6,0	12,0	-	0,1	-	8,90
ЖС47	2,5	-	2,0	1,3	9,3	8,8	5,57	11,0	-	-	0,02Y 0,02Ce 0,02La	9,089
Fourth generation												
ВЖМ4	2,5	-	4,0	4,0	6,0	4,5	6,0	6,0	-	-	0,02Y 0,02Ce 0,02La	8,879
MC-NG	4,0	0,5	1,0	5,0	4,0	5,0	6,0	-	-	0,1	4,0Ru 0,1Si	8,75
TMS-138	3,2	-	2,8	5,9	5,0	5,6	5,9	5,8	-	0,1	2,0Ru	8,95
TMS-138A	3,2	-	2,8	5,6	5,8	5,6	5,7	5,8	-	0,1	3,6 Ru	9,02
EPM-102 (MX-4)	2,0	-	2,0	6,0	5,95	8,25	5,55	16,5	-	0,15	-	9,20
Fifth generation												
TMS-162	2,9	-	3,9	5,8	4,9	5,6	5,8	5,8	-	0,1	6,0 Ru	-
TMS-196	4,6	-	2,4	5,0	6,4	5,6	5,6	4,6	-	0,1	5,0 Ru	9,01

As an example, in Fig. 3 shows the structure of a single crystal with a reduced density after heat treatment and casting of a GTE blade.

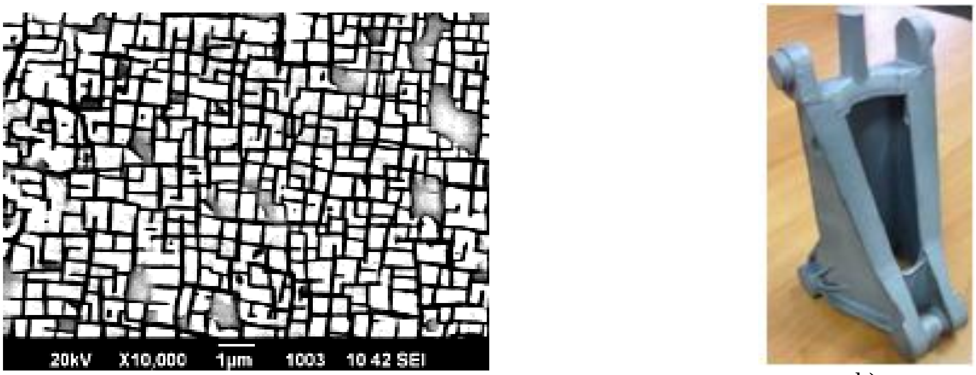

a) b)

Fig. 3. - Microstructure of single-crystal castings from an alloy of reduced density (a) and a blade of gas turbine engine (b) [21]

2. Steel surface

To date, the physical chemistry of common steels is associated with their complexes of mechanical and chemical properties. This is achieved by changing the concentration of carbon and alloying chemical elements, through various influences on the technology of casting and processing of finished steel parts. The main factor that affects the operation of parts in aviation and mechanical engineering is the properties of the surface and surface layer [22]. For aircraft parts, a surface layer is a layer in which the phase and chemical state are different from the material from which the part is made. On Fig. 4a shows the scheme of the surface layer of the metal with the interpretation of the layers [23]. In what follows, we will consider transition layer 3, assuming the absorbed and oxide layers to be remote. We also will not take into account the roughness of the metal shown in Fig. 4b. The operation of aircraft parts in difficult conditions: the implementation of flights at supersonic speeds, which are accompanied by "shock shocks" and aerodynamics of external force, a lot of repeated loads, flight modes in bad weather and non-climatic situations, in conditions of sudden temperature changes, forces the use of new approaches to the choice of materials for aircraft industry. This is especially important for civil aviation aircraft parts, where, first of all, it is necessary to increase the resource and cost, flight safety, and reduce the environmental impact [24]. Modern conditions, when choosing materials for aircraft construction, use a conceptual apparatus, which basically contains the concept of the integrated quality of the material. Such a concept includes such important parameters as weight efficiency, reliability, controllability, and others [24].

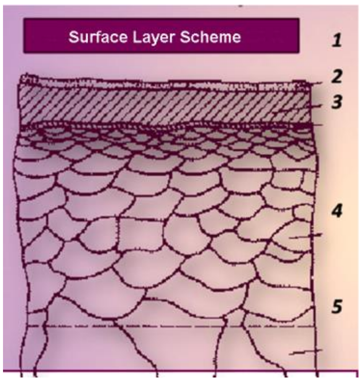

1 - adsorbed layer
2 - oxide layer (1-10 microns)
3 - transition layer (10-30 nm)
4 - technological layer (several mm)
5 - base metal

a)

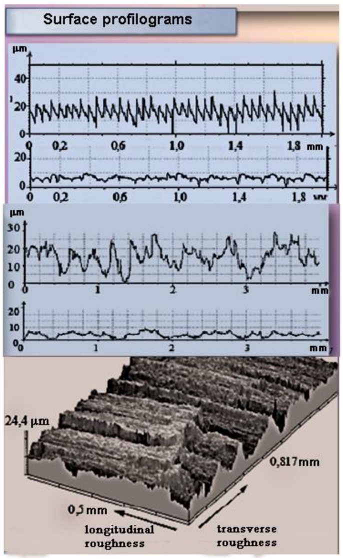

b)

Fig. 4. - Scheme of the surface layer (a), surface roughness (b)

Weight efficiency is mainly related to parameters that include strength and stiffness, specific strength, acoustic strength, and more. Since scientific and technological progress does not stand still both in fundamental research and in applied sciences, aviation technology is based both on completely new materials (which we talked about above) and surface modifications of new and old materials (Fig. 5).

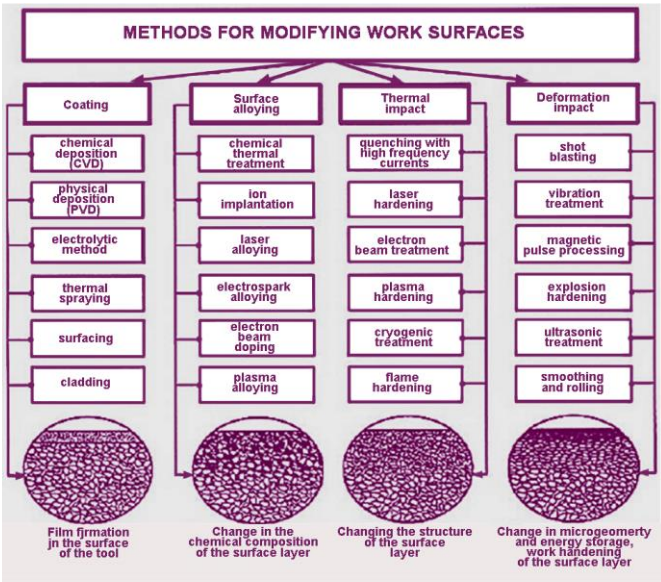

Fig. 5. - Methods for modifying the surface of parts

As an example, surface modification by an electron beam is shown in Fig. 6, and its microstructure is shown in Fig. 7.

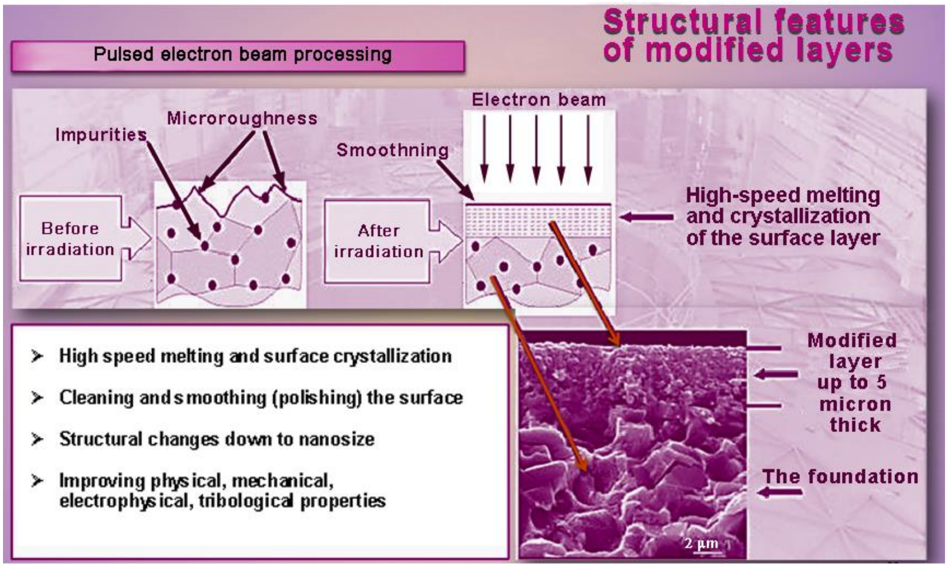

Fig. 6. - Electron beam melting

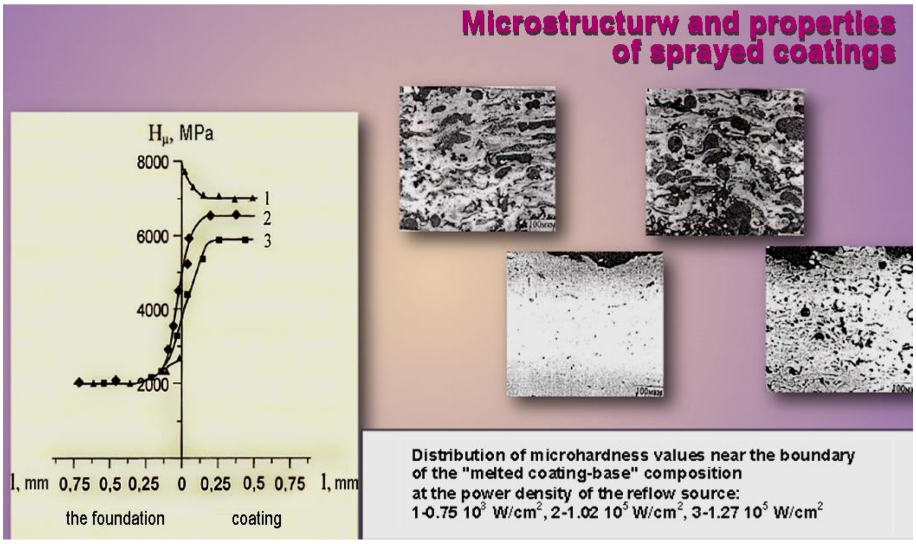

Fig. 7. - Microstructure of coatings

The components of iron-carbon alloys include iron, carbon and cementite. The following phases exist in the "iron-carbon" system: ferrite, austenite, perlite and ledeburite. The crystal lattice and microstructure of iron-carbon alloys are shown in fig. 8, 9.

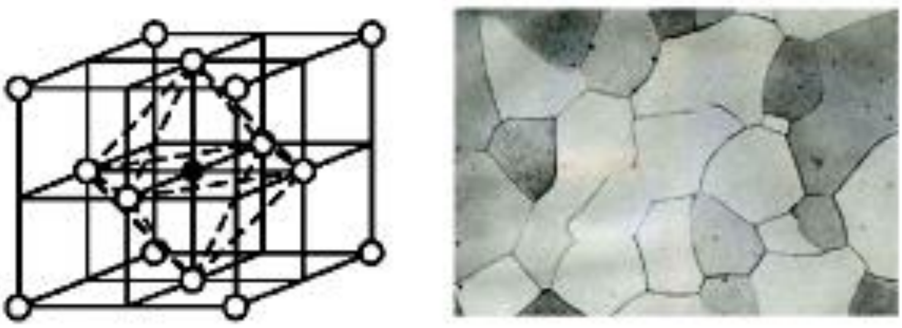

Fig. 8. - Crystal lattice and microstructure ferrite, x 500 [25]

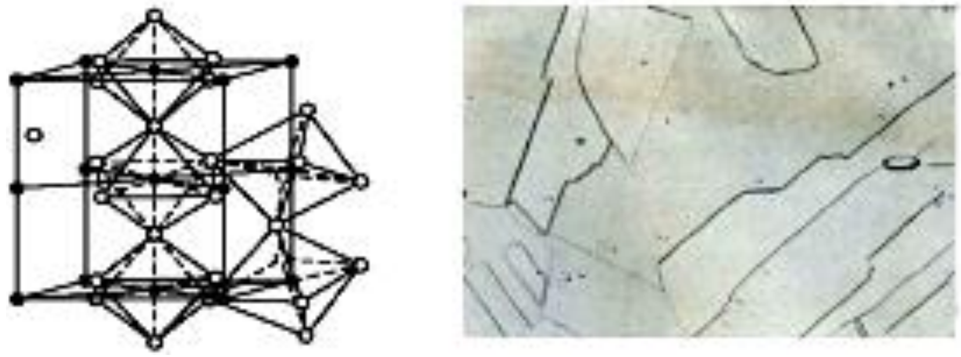

Fig. 9. - Crystal lattice and microstructure austenite, x 500 [25]

Heat-resistant alloys used for the manufacture of nozzle and working blades of gas turbines are complexly alloyed multicomponent nickel-based systems (Table 2). The influence of each alloying element in high-temperature nickel alloys is multifaceted. The same chemical component can simultaneously be a carbide-forming element and be part of a solid solution, increasing its strength.

3. Description of the empirical model

In [26], when considering the melting temperature of small particles, we obtained the following equation:

$$T(r) = T_0\left(1 - R(I)/r\right), \tag{1}$$

where the parameter R(I) is determined by the expression:

$$R(I) = 2\sigma\upsilon/RT, \tag{2}$$

where σ is the surface energy, υ is the molar volume, R is the universal gas constant, T is the temperature.

Experimental studies carried out by us with physical objects on thin films of various nature: mechanical, optical, magnetic [27], as well as the results of other researchers [25], showed the size dependence of all physical properties of small particles and thin films. This dependency looks like this:

$$\grave{A}(r) = \grave{A}_0\left(1 - R(I)/r\right), \tag{3}$$

where A(r) is a physical property (mechanical, etc.), which depends on the linear size (size effect), A_0 is a physical property (volumetric), which does not depend on the size.

Equations (1), (2), and (3) have the same structure and diverge as r → 0; therefore, we extend the definition of equation (3) and write it down finally:

$$\begin{aligned} &\grave{A}(r) = \grave{A}_0\left(1 - R(I)/r\right), \quad r >> R(I), \\ &A(r) = A_0\left(1 - R(I)/R(I) + r\right), \quad R_0 \le r \le R(I). \end{aligned} \tag{4}$$

This model is shown schematically in Figure 10. It is an ideal atomically smooth single crystal without vacancies, dislocations, and other defects.

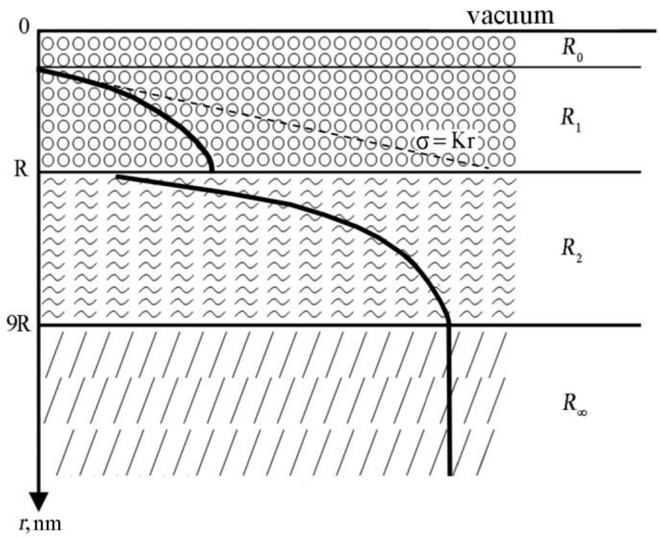

R_0 - de Broglie layer; R_1 - R(I) layer; R_2 - R(II) layer; R_∞ - massive sample layer

Fig.10. - Schematic representation of the surface layer [26]

The de Broglie layer $R_0=\lambda dB=\hbar/p$ for metals is from 0.01 nm to 0.1 nm. Quantum size effects begin in this layer. The main quantum-dimensional structures include structures with a two-dimensional electron gas - epitaxial films, MIS structures, heterostructures, etc.; structures with one-dimensional gas - quantum threads or wires; structures with zero-dimensional gas – quantum dots, boxes, crystallites [29].

The R(I) layer is described by the first dependence from Eq. (9) (r >> R(I)). In the R(I) layer with pure metal atoms, reconstruction and relaxation occur, associated with the restructuring of the surface [30]. For gold, the lattice constant is R(I) = 0.41 nm and the surface is rearranged at a distance $R(I)_{Au}=1.2/0.41\approx3$ of three atomic monolayers. Size effects in the R(I) layer are determined by the entire group of atoms in the system (collective processes). Such "quasi-classical" size effects are observed only in nanoparticles and nanostructures.

The R(II) layer extends approximately to the size $R(II)\approx9R=R\infty$, where the bulk phase begins. Dimensional properties start from this dimension. Nanomaterials are commonly understood as materials whose main structural elements do not exceed the nanotechnological boundary of ~100 nm, at least in one direction [31]. A number of researchers express the opinion that the upper limit (maximum size of elements) for nanostructures should be associated with a certain critical characteristic parameter: the mean free path of carriers in transport phenomena, the size of domains/domain walls, the diameter of the Frank-Read loop for dislocation glide, etc. [32-34]. This means that in the R(II) layer there should be many dimensional effects associated with optics, magnetism and other physical properties according to equation (4). The layer R(II) is described by the second dependence from equation (4) ($R_0<r<R(I)$). The parameter R(I) is related to the surface tension σ by formula (2). In [26], we have shown that, with an accuracy of 3%, the relation is fulfilled:

$$\sigma = 10^{-3} \cdot T_m, . \tag{5}$$

where T_m is the melting point of the solid (K).

The ratio is valid for all metals and for other crystalline compounds. At T=Tm from equation (2) we get:

$$R(I)_{ì} = 0{,}24 \cdot 10^{-9}\upsilon . \tag{6}$$

Equation (6) shows that the thickness of the surface layer R(I) is determined by one fundamental parameter - the molar (atomic) volume of the element $\upsilon=M/\rho$, M is the molar mass (g/mol), ρ is the density (g/cm^3), which periodically changes in accordance with the table D.I. Mendeleev. In [35] Rusanov A.I. at a constant temperature and phase composition (α) at small r, obtains the following linear dependence:

$$\sigma = K \cdot r , \tag{7}$$

where K is the proportionality factor depending on the temperature and composition of the phase (α) (see Fig. 10 layer R(I)). It follows from equation (7) that in the region of small radii of curvature, regardless of the specifics of the system, the surface tension always decreases with a decrease in the radius of curvature and becomes equal to zero when the radius of curvature of the tension surface vanishes. Let's compare formulas (5) and (7):

$$\sigma = \hat{E} \cdot R(I) = \cdot 10^{-3} \cdot T_m \,. \tag{8}$$

Where do we get:

$$\begin{aligned} \hat{E} &= 10^{-3} \cdot T_m / R(I) \\ \sigma &= 10^{-3} \cdot T_m / R(I) \cdot r \end{aligned}. \tag{9}$$

Here T_m is the melting temperature of the nanostructure: $\upsilon=M/\rho$, M is the molar mass (g/mol), ρ is the density (g/cm^3). The presence in equation (9) of the coordinate r(x, y, z) or r(a, b, c) leads to surface tension anisotropy. Finally we have:

$$\begin{aligned} &R(I)_{x=a} = 0{,}54 \cdot 10^{-11} \cdot x(a)^3, R(I)_{y=b} = 0{,}54 \cdot 10^{-11} \cdot y(b)^3, R(I)_{z=c} = 0{,}54 \cdot 10^{-11} \cdot z(c)^3, \\ &\sigma_a = 10^{-3} \cdot T_m \cdot R_a(I)/R(I), \sigma_b = 10^{-3} \cdot T_m \cdot R_b(I)/R(I), \sigma_c = 10^{-3} \cdot T_m \cdot R_c(I)/R(I). \end{aligned} \tag{11}$$

For equiatomic solid solutions, the following relations are valid:

$$T_m = \sum_{i=1}^{n} c_i (T_m)_i, M = \sum_{i=1}^{n} c_i (M)_i, \rho = \sum_{i=1}^{n} c_i (\rho)_i. \tag{12}$$

where $(T_m)_i$ is the melting point of each alloy element (K), $(M)_I$ is the molar mass of each alloy element (g/mol), ρ is the density of each alloy element (g/cm^3), c_i is the concentration of each alloy element, n is the number of alloy elements. Calculations of the surface energy will be carried out according to the formula derived under the assumption that there are no phase transitions of the first kind for these substances up to their melting point [36]:

$$\sigma_{hkl} = \left(\frac{\rho l_{hkl}}{M}\right) \int_o^{T_m} c_p dT. \tag{13}$$

where ρ is the density of the crystalline substance, and M is its molecular weight, T_m is the melting point, cp is the molar heat capacity, l_{hkl} is the thickness of the first coordination sphere in the [hkl] direction, which for crystals with body-centered (bcc) and face-centered (fcc)) cubic structure is given by the relations [36]:

$$\begin{aligned} &\text{Im3m, } Z = 2;\ l_{100} = a;\ l_{110} = a\sqrt{2};\ l_{111} = a/\sqrt{3}, \\ &\text{Fd3m, } Z = 4;\ l_{100} = a;\ l_{110} - a/\sqrt{2};\ l_{111} = 2a/\sqrt{3}. \end{aligned} \tag{14}$$

4. Calculation results and their discussion

Table 3 shows the values of the thickness of the surface layer and the surface energy of the steel parts of the aircraft industry. Shown here are steels VNS-2-Sh, VNS-25 and EP817, which are corrosion-resistant martensitic steels. Martensitic steels are distinguished by high hardness and strength, and this is explained by the fact that the martensite structure, being non-equilibrium, is characterized by the presence of strong internal stresses. In martensitic steels, when they are heated, carbon atoms are redistributed. This phenomenon is of a diffusion nature. As a result of this distribution, two phases are formed in the steel structure, each of which differs in carbon content and the shape of its crystal lattice.

Such phases, which are characterized by all steels of the martensitic class during their heating, are:

- ferrite, which contains a very small amount of carbon - up to 0.02% (elementary cells of the crystal lattice of ferrite have a BCC structure; the rest of the space in such cells is occupied by carbon);

- cementite, in which the carbon content is much higher - up to 6.67% (the rhombic crystal lattice of cementite is formed by unit cells having the shape of a rectangular parallelepiped).

In our calculations, we use the bcc structure and formulas (12) - (14).

Table 3. The thickness of the surface layer and the surface energy of steel parts in the aircraft industry

Steel	(hkl)	Structure	T_m, K	R(I), nm	σ_{hkl}, mJ/m^2
VNS-2-Sh	(100)	BCC	1887	1,7	1887
	(110)			1,2	1348
	(111)			1,0	1110
VNS-25	(100)	BCC	1807	1,6	1807
	(110)			1,1	1291
	(111)			0,9	1063
EP817	(100)	BCC	1836	1,6	1836
	(110)			1,1	1311
	(111)			0,9	1080

The thickness of the surface layer in Table 3 is about 1.7 nm for the (100) face, which coincides with the thickness of the surface layer of iron - R(I)=M/ρ = 1.7 nm, since iron in these steels is more than 70%. Considering that the parameter of the cubic body-centered lattice of iron is a = 0.2866 nm, the R(I) layer contains 1.7/0.2866 ≈ 6 iron monolayers, which undergo surface reconstruction or relaxation in this layer.

The diffusionless martensitic transformation has been considered both in theory and experimentally. It is shown that it can be described, like twinning, as a result of the motion of partial dislocations (since a full dislocation does not change the lattice). The movement of dislocations is, in fact, plastic deformation associated with surface energy during the crystallization of the alloy.

Table 3 shows that the geometry of movement of partial dislocations is associated with orientational crystallographic relations (the main one is "Kurdyumov-Sachs": planes (111)A // (101)M, and directions [110]A // [111]M. In the plane [111] the lowest value of the surface energy (Table 3).

Table 4 shows the corresponding values for nickel alloys.

Table 4. The thickness of the surface layer and the surface energy of nickel alloys in the aircraft industry

Alloy	(hkl)	Structure	T_m, K	R(I), nm	σ_{hkl}, mJ/m^2
First generation					
ЖС30М	(100)	HCC	1778	1,9	1778
	(110)			1,4	1270
	(111)			2,2	2092
ЖС40	(100)	HCC	1851	1,9	1851
	(110)			1,4	1322
	(111)			2,2	2178
Second generation					
ЖС36	(100)	HCC	1944	2,1	1944
	(110)			1,5	1389
	(111)			2,5	2287
Third generation					
ЖС47	(100)	HCC	2130	2,2	2130
	(110)			1,6	1521
	(111)			2,6	2506
Fourth generation					
ВЖМ4	(100)	HCC	2017	2,1	2017
	(110)			1,5	1441
	(111)			2,5	2373
Fifth generation					
TMS-196	(100)	HCC	2077	2,2	2077
	(110)			1,6	1484
	(111)			2,6	2444

The average thickness of the surface layer of nickel alloys is R(I) ≈ 2 nm, and the number of monolayers is 2/0.3524 ≈ 6. This value coincides with the number of iron monolayers. The average value of the surface energy of nickel alloys is greater than that of iron-based alloys. The structure of nickel-based alloys, like all alloys, is determined by the temperature gradient in the crystallization region, as well as the crystallization rate, which, in turn, depends on the magnitude of the surface energy, which determines the conditions for heat removal from the growing alloy during crystallization. Let us now consider the microhardness of steel (SS) coatings, high-entropy (HEA) coatings, and metallic glasses (MS) and their friction coefficients.

Table 5. Hardness and friction of NS, VES and MS coatings

NS	μ, HV	k	HEA	μ, HV	k	MS	μ, HV	k
ВНС-2Ш	279	0,43	CrNiTiZrCu	880	0,04	-	-	-
ВНС-25	282	0,50	FeCrNiTiZrAl	585	0,06	$Fe_{80}B_{20}$	1100	0,25
ЭП817	382	0,55	CoCrFeNiMn	659	0,05	$Fe_{78}Mo_2B_{20}$	1015	0,28
ЖС30М	240	0,38	CrNiTiZrCu	890	0,04	$Fe_{40}Ni_{40}P_{14}B_6$	640	0,19
ЖС40	280	0,42	AlTiVFeNiZr	800	0,07	$Fe_{78}P_{13}C_7$	760	0,21
ЖС36	250	0,52	MoTiVFeNiZr	740	0,12	$Fe_{78}Si_{10}B_{12}$	890	0,26
ЖС47	330	0,60	CuTiVFeNiZrCo	630	0,15	$Ni_{75}Si_8B_{17}$	860	0,30
ВЖМ4	334	0,53	MoTiVFeNiZrCo	790	0,18	$Co_{75}Si_{15}B_{10}$	910	0,29
TMS-196	362	0,45	AlTiVFeNiZrCoCr	780	0,23	$Ti_{50}Be_{40}Zr_{10}$	730	0,23

Table 5 shows that the hardness of high-entropy (HEA) coatings and metallic glasses (ML) are approximately the same, but almost 2 times higher than the hardness of steel coatings. For HEAs and MS coatings, the thickness of the surface layer is presented in Table 6 and is also approximately the same.

Table 6. Thickness of the surface layer of HEAs and MS coatings

HEA	R(I), nm	MS	R(I), nm
CrNiTiZrCu	1,4	$Fe_{78}Mo_2B_{20}$	1,3
FeCrNiTiZrAl	1,3	$Mg_{65}Cu_{25}Y_{10}$	1,8
CoCrFeNiMn	1,8	$Pd_{40}Ni_{40}P_{20}$	1,4
CrNiTiZrCu	1,7	$Fe_{78}Si_{10}B_{12}$	1,2
AlTiVFeNiZr	1,6	$Ti_{50}Be_{50}Zr_{10}$	1,7
MoTiVFeNiZr	1,4	$Fe_{40}Ni_{40}P_{14}B_6$	1,2
CuTiVFeNiZrCo	1,7	$Ni_{49}Fe_{29}P_{14}B_6Al_2$	1,2
MoTiVFeNiZrCo	1,8	$Zr_{62}Cu_{22}Al_{10}Fe_5Dy_1$	1,9
AlTiVFeNiZrCoCr	1,9	$Zr_{41.2}Ti_{13.8}Cu_{12.5}Ni_{10}Be_{22.5}$	1,6

In our opinion, there is much in common between high-entropy alloys and metallic glasses (Figs. 11 and 12).

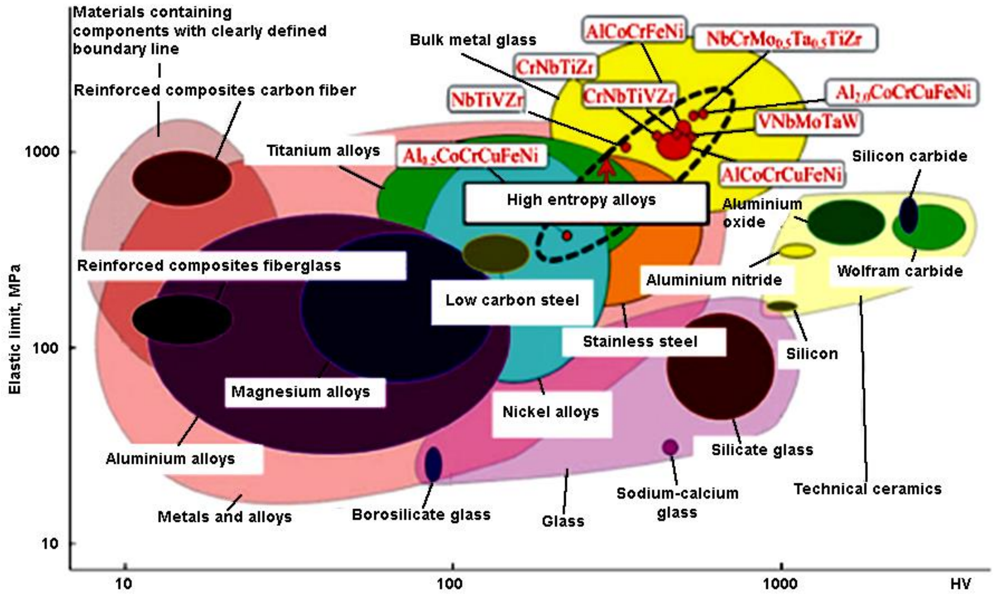

Fig. 11. - Correlation of the elastic limit and Vickers hardness for composites, ceramics, glasses, metal and high-entropy alloys [37]

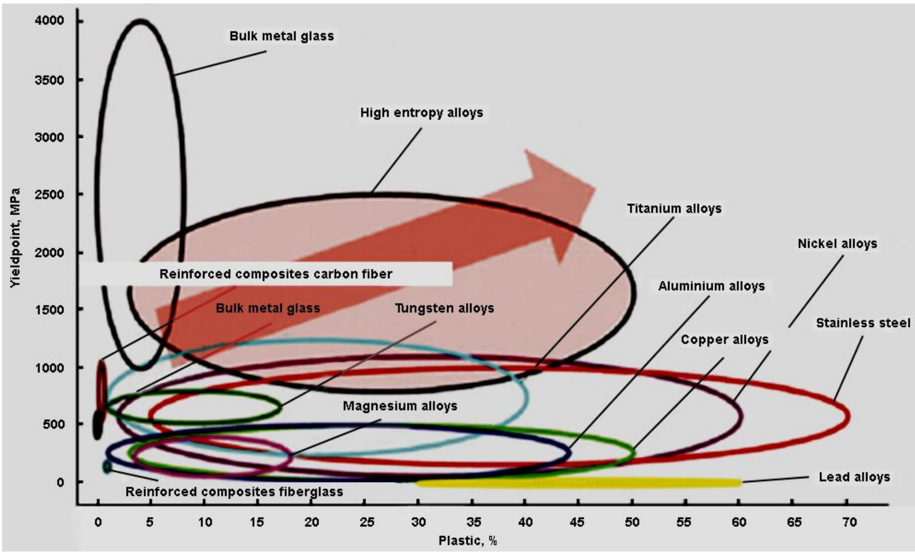

Fig. 12. - Correlation of yield strength and plasticity (tensile and compressive deformation at room temperature) for composites, ceramics, glasses, metal and high-entropy alloys [37]

It should be noted that the thickness of the surface layer equal to R(I) = M/ρ for HEAs and MSs is much lower than for structures with 4–5 or more elemental compositions (Table 7) [26]. Table 7 shows that the thickness of the surface layer R(I) of the most common crystals is an order of magnitude greater than the thickness of the surface layer of high-entropy alloys.

Table 7. The thickness of the surface layer of complex crystals [26]

Pomegranate group	R(I), nm	Pomegranate group	R(I), nm
$Mg_3Al_2(SiO_4)_3$	25,9	$Ca_3Fe_2Si_3O_{12}$	21,1
$Fe_3Al_2(SiO_4)_3$	19,7	$Ca_3Ti_2(Fe_2Si)O_{12}$	22,7
$Mn_3Al_2[SiO_4]_3$	19,6	$Ca_3Fe_2(SiO_4)_3$	18,8
$Ca_3Al_2[SiO_4]_3$	21,7	$Ca_3(VAlFe)_2(SiO_4)_3$	26,2

The first $Au_{75}Si_{25}$ metallic glass was obtained by an American group in the USA in 1960 [38], and the first high-entropy alloy was obtained by Chinese researchers in 2004 [39], that is, 40 years later than metallic glasses.

Researchers identify 4 main features of HEA [39]:

1) high entropy of mixing;
2) distortion of the crystal lattice;
3) slow diffusion;
4) mixing effect.

In review [38], a list of five main models of the structure of amorphous alloys currently under consideration is given, but there is no final model yet.

1. A model that treats rigid spheres as chaos when they are packed. Since the actual density of metallic glasses is about 5% lower than that of the corresponding crystal structures, this model is not realistic.

2. Packing model for polyhedra. The model considers polytetrahedral packing, which assumes the packing density of rigid sphere density polyhedra.

3. Stereochemical model. Due to the fact that the strongest interaction occurs between nearby atoms, it is possible to consider metallic glasses as solids with short-range order, as happens in real crystals, with the only difference that metallic glasses allow some disorder. This model is valid for some metallic glasses, but is poorly applicable to many amorphous alloys.

4. Efficient Packing Model for Quasi-Equivalent Clusters. The model is based on considering the structure as some packing of clusters with a short-range order characteristic of the given alloy. Moreover, the coordination polyhedron, which is formed from neighboring atoms, creates a local environment without pores between clusters. This model is applicable to metallic glasses consisting of pure metals.

5. Model of the average order or packing by fractals. This model shows that the average order in metallic glasses is described by the theory of fractals. These works are just getting started.

We emphasize once again that, in our opinion, there is much in common between high-entropy alloys and metallic glasses. Now let's turn to Table 5, namely, the coefficient of friction k. The friction of steel and nickel coatings lies at the level of 0.4-0.6. The coefficient of friction of multi-element nitride (μ ~ 0.96) turned out to be slightly higher than that of TiN- (μ ~ 0.84) and metallic (μ ~ 0.87) coatings. For metallic glasses, the coefficient of friction is higher than 0.2 or more. For WESs, the coefficient of friction is much less than 0.1. What is the reason for this difference? In [40], within the framework of the thermodynamic approach, we obtained the following formula for the coefficient of dry friction:

$$k = \tilde{N}\cdot\grave{O}\cdot\frac{\sigma\cdot S}{\Delta G^0}\cdot\overline{N}, \tag{15}$$

where σ is the specific surface energy of the material, S is the contact area, T is the temperature, ΔG^0 is the Gibbs energy, N is the average number of elementary destruction carriers (proportional to the number of defects), C is a constant. But according to the molecular kinetic theory, the friction force F ~ k is equal to:

$$F = \int \sigma dL \approx \sigma\cdot L, \tag{16}$$

where σ is the surface energy (Table 2), L is the length of the traveled path.

Equation (16) shows that the friction coefficient is proportional and increases with increasing surface energy according to (16), that is, the value of σ from Table 2 should lead to an increase in the friction coefficient. But the reverse picture is observed experimentally, the friction coefficient decreases, which contradicts the molecular kinetic theory, but becomes explainable from the point of view of our formula (16), which contains the Gibbs formula in the denominators.

Considering the case where an alloy is formed from its constituent elements under isobaric conditions, the change ΔG_{mix} of mixing from the initial elemental state to the state after fusion can be expressed as:

$$\Delta G_{mix} = \Delta H_{mix} - T\Delta S_{mix}. \tag{17}$$

An equilibrium state is a state at a minimum of free energy. On fig. 13a shows an increase in the entropy of mixing with an increase in the number of elements for equimolar alloys. It can be seen that the entropy of mixing for solid solution phases increases from a small value for ordinary alloys to a large value for high-entropy alloys of the composition [41].

Based on the effect of the entropy of mixing, it is possible to divide the variety of alloys into three fields, as shown in Fig. 7b. Low entropy alloys are traditional alloys. High-entropy alloys are alloys with at least five main elements. Medium entropy alloys are alloys with 2…4 main elements. The high-entropy effect of activating the appearance of a disordered solid phase essentially occurs in the field of high-entropy alloys and should be present to a lesser extent in medium-entropy alloys. Stabilization of a simple solid solution phase is important for the microstructure and properties that can be obtained in these materials [41].

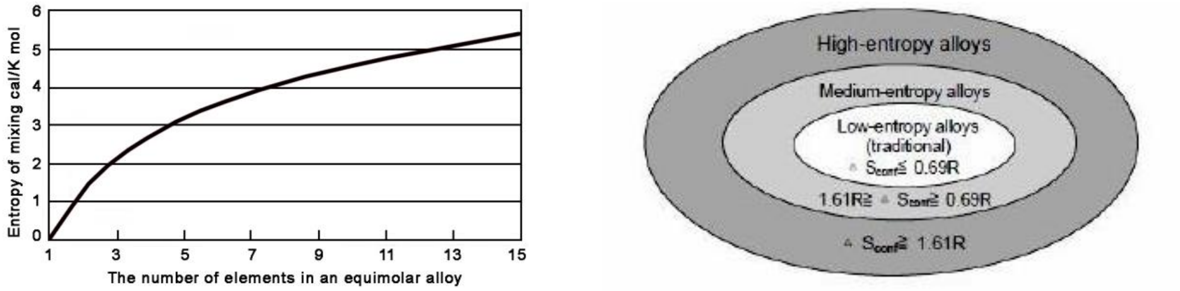

a) b)

Fig. 13. Increment of the entropy of mixing by the number of elements in equimolar alloys in a disordered state (a), division of the world of alloys by the entropy of mixing (b) [41]

Since tribological properties play a significant role in engineering, high-entropy alloys and coatings will take their rightful place among structural materials. For example, in the aerospace industry, in which the issue of creating tribological coatings with a low coefficient of friction under changing operating conditions (temperature, humidity, pressure, atmosphere) is fundamental for further progress and the development of a new type of equipment. Spacecraft have a large number of moving parts: flywheels, gyroscopes, antenna and solar array drives, pumps, gears [42]. All these parts are subjected to different loads and friction velocities from values close to zero to 20 m/s in gyroscopic systems. For example, bearings used in gyroscope gimbals for fast positioning of spacecraft in orbit rotate at a frequency of up to 500 Hz when performing maneuvers. It should be noted that in addition to high loads and rotational speeds, parts are subject to changing operating conditions: exposure to moisture during assembly and launch of aircraft, exposure to an oxidizing atmosphere when passing through the Earth's atmosphere, temperature fluctuations from -100 ° C to 100 ° C in orbit and heating up to 1000 °C when entering the atmosphere. Requirements for mechanical characteristics, performance in various conditions, service life of products for the aerospace industry currently exceed the capabilities of existing anti-friction materials, which necessitates the development and implementation of advanced materials and technologies. So at the moment there is no antifriction material that works stably in a wide temperature range from 25 to 1000 °C, although this circumstance is a key point for the further development and production of high-speed aircraft jet engines and small-sized engines operating without cooling systems for aerospace vehicles. Therefore, in recent years there has been a great interest in the development of thin coatings to reduce friction and wear of working surfaces, not only from scientists, but also from enterprises of the military-industrial and aerospace complex. In this regard, many works in this direction are closed. Recent advances in the field of ion-plasma technologies make it possible to deposit coatings with desired properties that were unattainable even five to ten years ago. Examples include multiphase coatings of the "chameleon" type [43] and multilayer coatings [44] with unique mechanical and chemical properties.

Conclusion

In aircraft construction, steel and nickel alloys still remain the basis of structural materials. The results presented in the article show that the hardness of high-entropy (HEA) coatings and metallic glasses (ML) is approximately the same, but almost 2 times higher than the hardness of steel and nickel coatings. For HEAs and MS coatings, the thickness of the surface layer is also approximately the same. In our opinion, there are many similarities between high-entropy alloys and metallic glasses. Equation (16) shows that the friction coefficient is proportional and increases with increasing surface energy according to (16), that is, the value of σ from Table 2 should lead to an increase in the friction coefficient. But the reverse picture is experimentally observed, the friction coefficient decreases, which contradicts the molecular kinetic theory, but becomes explainable from the point of view of our formula (16), which contains the Gibbs formula in denominators, which decreases for high-entropy alloys. Thus, high-entropy coatings can be used in aircraft construction due to their high hardness and low friction coefficient.

Acknowledgments

This research was funded by the Committee of Science of the Ministry of Science and Higher Education of the Republic of Kazakhstan (grant URN AR14972877 «Development of methods for forecasting sudden emissions of coal and gas based on the study of coal nanocoating»/

References

[1] Yurov V.M., Oleshko V.S. The impact of the environment on the contact potential difference of metal machine parts. Eurasian Physical Technical Journal, 2019. Vol.16, No.1(31), pp. 99 – 108.
[2] Yurov V.M., Makeeva O.V., Oleshko V.S., Fedorov A.V. Development of a device for determining work electron output. Eurasian Physical Technical Journal, 2020, Vol.17, No.1 (33), pp. 127 – 131.
[3] Yurov V.M., Goncharenko V.I.,Oleshko V.S. Anisotropy of the surface of cubic body-centered crystal lattices. Eurasian Physical Technical Journal, 2021, Vol.18, No.1(35). – P. 9-15.
[4] Strategy for the development of the aviation industry of the Russian Federation for the period up to 2030 [Electronic resource]: Ministry of Industry and Trade of the Russian Federation - access mode: http://minpromtorg.gov.ru/docs.
[5] Kablov E.N. Innovative developments of the Federal State Unitary Enterprise "VIAM" of the State Scientific Center of the Russian Federation for the implementation of the "Strategic Directions for the Development of Materials and Technologies for Their Processing for the Period until 2030" // Aviation Materials and Technologies, 2015, No. 1(34). - P. 3-33.
[6] Skorobogatov S.V. A method for substantiating the requirements for newly created combustion chambers with a transverse vortex formation system for aircraft engines. - Dissertations for the degree of candidate of technical sciences, Moscow, 2020. - 153 p.
[7] Kuzmenko A.S. Methods, technologies and means of improving the quality and efficiency of aviation chemical work. - Dissertations for the degree of candidate of technical sciences, Taganrog, 2020. - 173 p.
[8] Glukhov G.E. The system of continuous information monitoring of the safety of aviation activities in the field of universal inspections of the international civil aviation organization. - Dissertations for the degree of candidate of technical sciences, Moscow, 2020. - 183 p.
[9] Volkov A.K. Development and research of models and algorithms for decision support in the tasks of ensuring aviation security. - Dissertations for the degree of candidate of technical sciences, Ulyanovsk, 2019. - 183 p.
[10] Amui ali Mohammad. A method for restoring the working capacity of GTE turbine blades through the use of an improved protective coating. - Dissertation. for the degree of candidate of technical sciences, Moscow, 2019. - 137 p.
[11] Nasteka V.V. Improving the performance properties of cast blades from heat-resistant nickel alloys due to surface nanostructuring. - Dissertation. for the degree of candidate of technical sciences, Ufa, 2019. - 118 p.
[12] Lopatkin R.V. Development of a business model for enterprises in the civil aircraft industry as part of the integration of corporate strategies and projects. - Dissertation. for the degree of candidate of economic sciences, Moscow, 2019. - 132 p.
[13] Klimov V.N., Kozlov D.M. Modern aviation structural alloys. - Samara: Publishing House of Samara University, 2017. - 40 p. [in Russian]
[14] Gromov V.I., Voznesenskaya N.M., Pokrovskaya N.G., Tonysheva O.A. High-strength structural and corrosion-resistant steels of FSUE "VIAM" for products of aviation equipment // Aviation materials and technologies, 2017, No. 8. - P. 159-174.
[15] Krylov S.A., Markova E.S., Shcherbakov A.I., Yakusheva N.A. Metallurgical features of the smelting of high-strength maraging steel VKS-180-ID // Aviation materials and technologies, 2015, No. 4(37). - P. 14–20.
[16] Kablov E.N. What is the future to be made of? New generation materials, technologies for their creation and processing - the basis of innovation // Wings of the Motherland, 2016, No. 5. - P. 8-18.
[17] Gromov V.I., Kurpyakova N.A., Korobova E.N., Sedov O.V. New heat-resistant steel for aircraft bearings // Proceedings of VIAM, No. 2(74), 2019. - P. 17-23.
[18] Kablov E.N., Svetlov I.L., Petrushin N.V. Nickel heat-resistant alloys for casting blades with a directed and single-crystal structure // Materialovedenie, 1997, No. 4. - P. 32-38; - No. 5. - P. 14-17.
[19] Kablov E.N., Muboyadzhyan S.A. Heat-resistant and heat-shielding coatings for high-pressure turbine blades of promising gas turbine engines // Aviation materials and technologies, 2012, No. 5. - P. 60-70.
[20] Petrushin N.V., Ospennikova O.G., Svetlov I.L. Monocrystalline heat-resistant nickel alloys for turbine blades of advanced gas turbine engines // Aviation materials and technologies, 2017, No. 8. – P. 72−103.
[21] Ospennikova O.G. Development of the scientific basis for the creation of a new generation of low-density cast heat-resistant nanostructured nickel alloys with the required set of mechanical properties. - Dissertations for the degree of Doctor of Technical Sciences, Moscow, 2018. - 321 p.
[22] Krivezhenko D.S. Structure and properties of surface layers formed by the method of non-vacuum electron-beam surfacing of a powder mixture containing boron carbide. - Dissertations for the degree of candidate of technical sciences, Novosibirsk, 2016. - 198 p. [in Russian]
[23] Stepanova T.Yu. Technologies of surface hardening of machine parts. - Ivan. state chemical-technological un-t.- Ivanovo, 2009. - 64 p. [in Russian]
[24] Kolganov I.M., Dubrovsky P.V., Arkhipov A.N. Manufacturability of aircraft structures, ways to improve. Part 1. - Ulyanovsk: UlGTU, 2003. - 148 p.
[25] Frolova O.S. Materials Science. - Yuzhno-Sakhalinsk: SakhGU, 2016. - 84 p. [in Russian]
[26] Yurov V.M., Guchenko S.A., Laurinas V.Ch. Surface layer thickness, surface energy and atomic volume of an element // Physico-chemical aspects of the study of clusters, nanostructures and nanomaterials, 2018, No. 10. - P. 691-699.
[27] Yurov V.M., Laurinas V.Ch., Guchenko S.A., Zavatskaya O.N. Dimensional effects and surface tension of pure metals // Successes of modern natural sciences, 2012. - No. 7. - P. 88-93.
[28] Kirchanov V.S. Nanomaterials and nanotechnologies. - Perm: Publishing House of Perm. nat. research polytechnic un-ta, 2016 - 193 p. [in Russian]
[29] Arutyunov K.Yu. Quantum size effects in metallic nanostructures // Dokl. RAN, 2015. No. 3(28). - P. 7-16.

[30] Oura K., Lifshitz V.G., Saranin A.A., Zotov A.V., Katayama M. Introduction to surface physics. - M.: Science. 2006. - 490 p. [in Russian]
[31] Uvarov N.F., Boldyrev V.V. Size effects in the chemistry of heterogeneous systems // Uspekhi khimii, 2001, V. 70(4). - P. 307-329. [in Russian]
[32] Gusev A.I. Nanomaterials, nanostructures, nanotechnologies. - M.: Fizmatlit, 2005. - 412 p. [in Russian]
[33] Andrievsky R.A., Ragulya A.V. Nanostructured materials. - M.: Publishing Center "Academy", 2005. - 192 p. [in Russian]
[34] Suzdalev I.P. Nanotechnology: physical chemistry of nanoclusters, nanostructures and nanomaterials. - M.: KomKniga, 2006. - 592 p. [in Russian]
[35] Rusanov A.I. Phase equilibria and surface phenomena. - L.: Chemistry, 1967. - 346 p. [in Russian]
[36] Bochkarev V.P. Development of physical and chemical principles for assessing the effect of surface energy on the properties of materials and processes for microelectronics technology. - Thesis for the degree of Doctor of Technical Sciences, Moscow, 2020. - 299 p.
[37] Tang Z., Gao M.C., Diao H., Yang T.F., Liu J.P., Zuo T.T., Shang Y., Lu Z.P., Cheng Y.Q., Zhang Y.W., Dahmen K.A., Liaw P.K., Egami T.. Aluminum Alloying Effects on Lattice Types, Microstructures, and Mechanical Behavior of High-Entropy Alloys Systems. // JOM, 2013, **65**. – P. 1848 – 1858.
[38] Cheng Y.Q., Ma E. (2011). Atomic-level structure and structure–property relationship in metallic glasses // Progress in Materials Science, Vol. 56. – P. 379–473.
[39] Yeh J.-W., Chen S.-K., Lin S.-J., Gan J.-Y., Chin Ts.-Sh., Shun T.-Ts., Tsau Ch.-H., Chang Sh.-Y. Nanostructured High-Entropy Alloys with Multiple Principle Elements: Novel Alloy Design Concepts and Outcomes // Advanced Engineering Materials, 2004, Vol. 6, №8. - P. 299-303.
[40] Yurov V.M., Laurinas V.Ch., Zavatskaya O.N. Tribological properties of ion-plasma coatings // Bulletin of KarSU. Physics, 2012. - No. 3(67). - P. 11-18.
[41] Yeh J.W., Chen Y.L., Lin S.J. High-entropy alloys – a new era of exploitation // Materials Science Forum, 2007, Vol. 560. – P. 1-9.
[42] Conley P.L., Packard D., Purdy W. Space vehicle mechanisms. – Wiley, 1998. – 794 p.
[43] Muratore C., Voevodin A.A. Chameleon Coatings: Adaptive Surfaces to Reduce Friction and Wear in Extreme Environments // Annual Review of Materials Research, 2009, V. 39. – P. 297–324.
[44] Kutschej K., Mayrhofer P.H., Kathrein M., Polcik P., Mitterer C. A new low-friction concept for $Ti_{1-x}Al_xN$ based coatings in high-temperature applications // Surface and Coatings Technology, 2004, V. 188-189. – P. 358-363.

Information of the authors

Yurov Viktor Mikhailovich, Candidate of Physical and Mathematical Sciences, Associate Professor, Karaganda Buketov University
e-mail: exciton@list.ru

Goncharenko Vladimir Ivanovich, Doctor of Technical Sciences, Professor, Director of the Military Institute, Moscow Aviation Institute (National Research University)
e-mail: fvo@mail.ru

Portnov Vassily Sergeevich, Doctor of Technical Sciences, Professor, Abylkas Saginov Karaganda Technical University
e-mail: vs_portnov@mail.ru

Sha Mingun, PhD, Professor, Northwestern Polytechnic University, Yangtze River Delta Research Institute of Northwestern Polytechnic University, Taicang, China
e-mail:sha.m@gmai.com

Oleshko Vladimir Stanislavovich, Candidate of Technical Sciences, Professor, Moscow Aviation Institute (National Research University)
e-mail: ovs_mai@mail.ru

Rakhimova Zhanara Baibolsynovna, Master of Technical Sciences, Assistant, Abylkas Saginov Technical University
e-mail: zhanara.rahimova.87@mail.ru

Rakhimov Murat Amanzholovich, Candidate of Technical Sciences, Associate Professor, Abylkas Saginov Technical University
e-mail: rahimov67@mail.ru

Rakhimova Galiya Mukhamedievna, Candidate of Technical Sciences, Associate Professor, Abylkas Saginov Technical University
e-mail: g.rakhimova@kstu.kz

Maussymbayeva Aliya Dumanovna, PhD, Associate Professor, Abylkas Saginov Technical University
e-mail: aliya_maussym@mail.ru

DOI 10.52209/2706-977X_2023_1_24 **IRSTI 55.33.39** **UDC 629.114.46(575.3)**

Influence of Pressure on Tire Wear of Mining Dump Truck

Khoroshavin S.A.[1,2*], Nekrasova O.S.[1]
[1] Ural State Mining University, Ekaterinburg, Russia
[2] Ural Federal University, Ekaterinburg, Russia
*corresponding author

Annotation. The article shows the dependence of ground pressure on the number of wheels and tire inflation pressure for dump trucks, the dependence of tire pressure, tire deformation and contact patch length on tire inflation pressure and tire temperature. Currently, some of the dump trucks in Russian quarries are operated in off-road conditions on soils with low bearing capacity. Work on weak soils requires the use of vehicles with high cross-country ability and low specific pressure on the ground. One way to improve off-road mobility is to use articulated dump trucks.

Keywords: mining dump truck, cross-country ability, calculation, ground pressure, tire wear, contact patch

Introduction

With this articulated dump truck can maneuver in a narrow space due to the small turning radius of the machine. Most of articulated dump trucks have capacity from 10 to 50 tons. In the former Soviet Union, production of articulated dump trucks is the responsibility of the Belarusian production association BelAZ, which produces three-axle model BelAZ-7528 and its modification BelAZ-75281 with a carrying capacity of 36 tonnes [5].

If there is a need to use machines with a higher payload capacity on weak soils, the option of using multi-bearing dump trucks is being considered. A dump truck with a multi-supported drive can continue to move even if the tires of some of the wheels are out of order [7]. The disadvantages of such design can include: less reliability and greater complexity of maintenance and repair of the transmission, in comparison with the transmission of classic dump trucks, the high cost of dump trucks with multi-supported running.

1. Degree of development of the topic

On wheeled dump trucks, you can change the specific pressure either by changing the tire inflation pressure or by increasing the number of dump truck wheels.

When loaded, a dump truck tire deforms (Fig. 1).

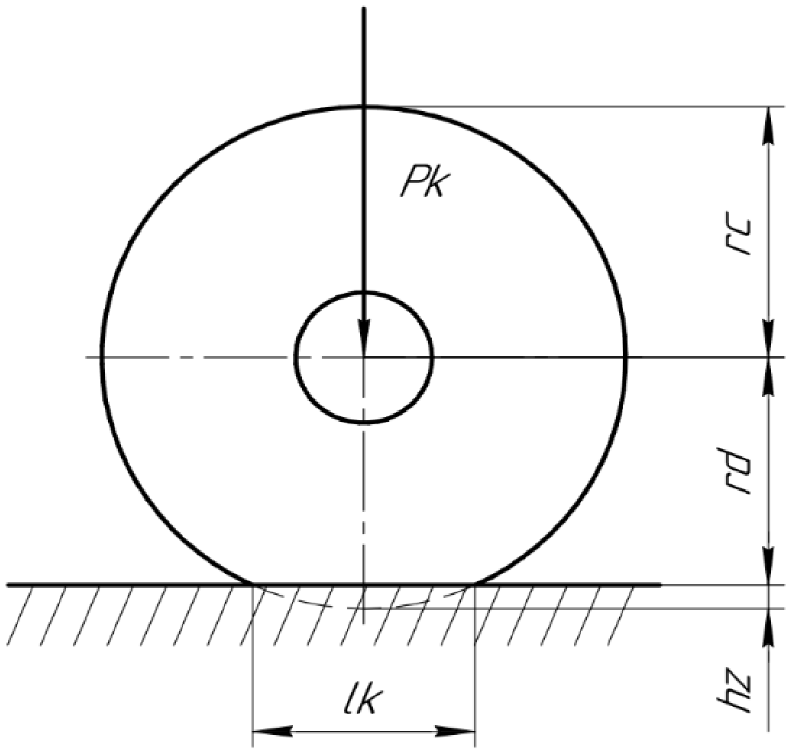

Fig. 1. - Calculation scheme for determining the contact area

The magnitude of the tire deformation h_z can be determined from the expression [1]:

$$h_z = \sqrt{\frac{K_z P_k^{\frac{3}{4}}}{1+P_w}} \tag{1}$$

where K_z - coefficient of vertical deformation of the tire from the load;

P_k – load on the tire, kN;

P_w – air pressure in the tire, kPa.

Contact area length of the wheel tire l_k [8]:

$$l_k = 2\sqrt{2r_c h_z - h_z{}^2} \tag{2}$$

where r_c – free radius of the tire above the axis of rotation, m.

The free radius of the tire can be assumed to be half the outside diameter of the unloaded wheel. The width of a wheel's tire contact patch area b_k is approximately equal to the width of the tire's racetrack. It is possible to accept [3, 4, 5, 6]:

$$b_k = (0{,}65\ldots0{,}75)B \tag{3}$$

where B - width of the tire profile, m.

Large truck tires are characterized by a rectangular contact patch shape. Then the wheel pressure on the ground P is defined as:

$$P = \frac{P_k}{l_k \cdot b_k} \tag{4}$$

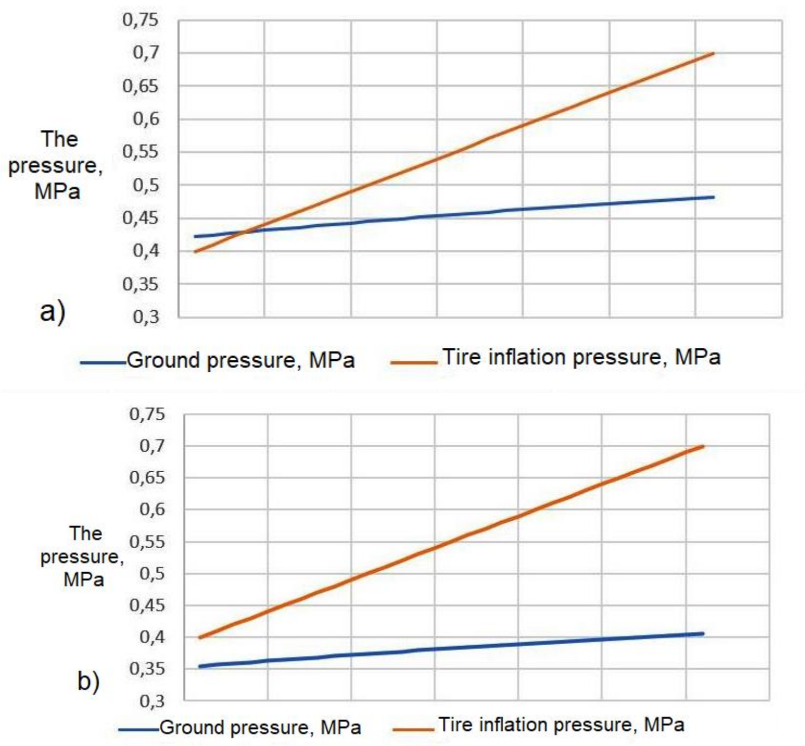

a) of BELAZ-75130, b) of a dump truck with a multi-point drive

Fig. 2. – Dependence of ground pressure on tire inflation pressure

Fig. 2 shows the calculated dependence of pressure on the ground, developed by BelAZ 75130 dump truck (6 wheels) and a similar in weight dump truck with multi-supported (eight pairs of wheels) on the inflation pressure of tires. As the number of wheels increases, the load per wheel, wheel diameter and width decreases. This leads to a decrease in the contact area of the wheel with the road. According to the results of calculations, we can conclude that multi-support dump trucks exert less pressure on the ground than dump trucks with a classic layout. When you increase the number of wheels by 2.7 times the pressure developed by the dump truck on the ground is reduced by 1.2 times. The developed pressure is not enough in order to consider this parameter as a distinct advantage of dump trucks with multipumped drive over conventional dump trucks, that limits the appropriateness of using dump trucks with multipumped drive in quarries with weak soils due to their high cost and complexity of maintenance. However, the multi-bearing course can be used when working in cramped conditions due to the high maneuverability of dump trucks with it.

2. Results

The pressure exerted by the dump truck on the ground is significantly affected by the air temperature in the tire, which depends, among other things, on the ambient temperature. Tables 1 and 2 show the calculated dependencies of tire pressure, tire deformation and contact patch length on tire inflation pressure and tire temperature.

Table 1. Dependence of tire pressure, tire deformation and contact patch length on tire inflation pressure and tire temperature for BELAZ-75130 dump truck

Pumping pressure, MPa	Parameter	Ambient temperature, ^{o}C							
		-30	-20	-10	0	10	20	30	40
0,4	Tire pressure, MPa	0,41	0,41	0,42	0,42	0,43	0,43	0,43	0,44
	Deformation, m	0,16	0,16	0,15	0,15	0,15	0,14	0,14	0,14
	Contact length, m	1,48	1,46	1,45	1,44	1,43	1,41	1,40	1,39
0,55	Tire pressure, MPa	0,37	0,38	0,38	0,38	0,39	0,39	0,39	0,40
	Deformation, m	0,09	0,09	0,09	0,09	0,09	0,09	0,08	0,08
	Contact length, m	0,87	0,86	0,86	0,85	0,84	0,84	0,83	0,82
0,7	Tire pressure, MPa	0,47	0,47	0,48	0,48	0,49	0,49	0,49	0,50
	Deformation, m	0,12	0,12	0,12	0,11	0,11	0,11	0,11	0,11
	Contact length, m	1,29	1,28	1,27	1,26	1,25	1,24	1,23	1,22

Table 2. Dependence of tire pressure, tire deformation and contact patch length on tire inflation pressure and tire temperature for a multi-position dump truck

Pumping pressure, MPa	Parameter	Ambient temperature, ^{o}C							
		-30	-20	-10	0	10	20	30	40
0,4	Tire pressure, MPa	0,34	0,35	0,35	0,35	0,36	0,36	0,36	0,37
	Deformation, m	0,11	0,11	0,11	0,10	0,10	0,10	0,10	0,10
	Contact length, m	0,94	0,93	0,92	0,92	0,91	0,90	0,89	0,89
0,55	Tire pressure, MPa	0,37	0,38	0,38	0,38	0,39	0,39	0,39	0,40
	Deformation, m	0,09	0,09	0,09	0,09	0,09	0,09	0,08	0,08
	Contact length, m	0,87	0,86	0,86	0,85	0,84	0,84	0,83	0,82
0,7	Tire pressure, MPa	0,39	0,40	0,40	0,41	0,41	0,41	0,42	0,42
	Deformation, m	0,08	0,08	0,08	0,08	0,08	0,08	0,07	0,07
	Contact length, m	0,82	0,82	0,81	0,80	0,79	0,79	0,78	0,78

When you change the pressure in the tire, the rate of tire wear changes. Using experimental data from open sources [9], a graph of the dependence of tire runability on inflation pressure was plotted (Fig. 3).

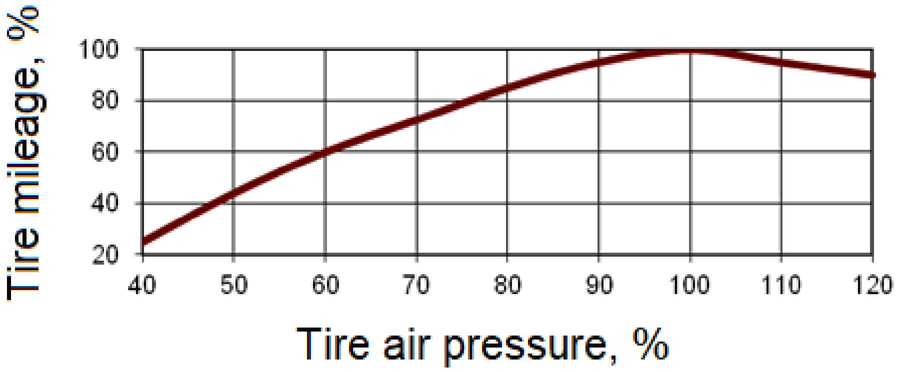

Fig. 3. – Dependence of tire runability on inflation pressure

The smallest error in approximating these values can be obtained by using a quadratic approximation. Regression analysis showed: the correlation coefficient when using quadratic approximation is 0.9982, the coefficient of determination (R-square) is 0.9965, the average error of approximation is 1.8769%. The coefficient of determination is close to one, which indicates the high accuracy of the proposed empirical expression for determining the tire wear of the vehicle depending on the pressure in the tire.

The mileage of a tire until it is completely worn out can be determined from an empirical expression:

$$L = -1{,}7L_{н} \cdot \left(\frac{P}{P_{н}}\right)^2 + 3{,}6L_{н} \cdot \frac{P}{P_{н}} - 0{,}9L_{н} \tag{5}$$

where P – tire pressure;

P_{H} – rated inflation pressure of the tire;

L_{H} – the nominal mileage of the tire before it is scrapped.

To determine the ratio of the tire's mileage to its nominal mileage, you can use the expression:

$$L_{\%} = -1{,}7\left(\frac{P}{P_{н}}\right)^2 + 3{,}6\frac{P}{P_{н}} - 0{,}9 \tag{6}$$

As the ambient temperature changes, the runability of the tire also changes. If we assume a temperature of 15°C as the nominal inflation temperature of the tire, the dependence takes the form (6,9):

$$L_{\%} = -1{,}7\left(\frac{P \cdot t}{t_{н}P_{н}}\right)^2 + 3{,}6\frac{P \cdot t}{t_{н}P_{н}} - 0{,}9 \tag{7}$$

where t – ambient temperature, K;

$t_{н}$ - air temperature when inflating the tire.

Table 3 and Fig. Table 3 shows the calculated dependences of the ratio of tire run to full wear to the nominal mileage on tire inflation pressure and tire temperature for BelAZ 75130 open-pit dump truck.

Table 3. Dependence of tire runability on inflation pressure and ambient temperature

Pumping pressure, MPa	Parameter	Ambient temperature, °C							
		-30	-20	-10	0	10	20	30	40
0,4	Pressure on ground, MPa	0,41	0,41	0,41	0,42	0,42	0,42	0,43	0,43
	Share of mileage to total wear and tear	0,67	0,71	0,74	0,78	0,81	0,84	0,86	0,89
0,55	Pressure on ground, MPa	0,44	0,44	0,45	0,45	0,45	0,46	0,46	0,46
	Share of mileage to total wear and tear	0,93	0,95	0,97	0,99	1,00	1,00	1,00	1,00
0,6	Pressure on ground, MPa	0,45	0,45	0,46	0,46	0,46	0,47	0,47	0,47
	Share of mileage to total wear and tear	0,97	0,99	1,00	1,00	1,00	1,00	0,99	0,98

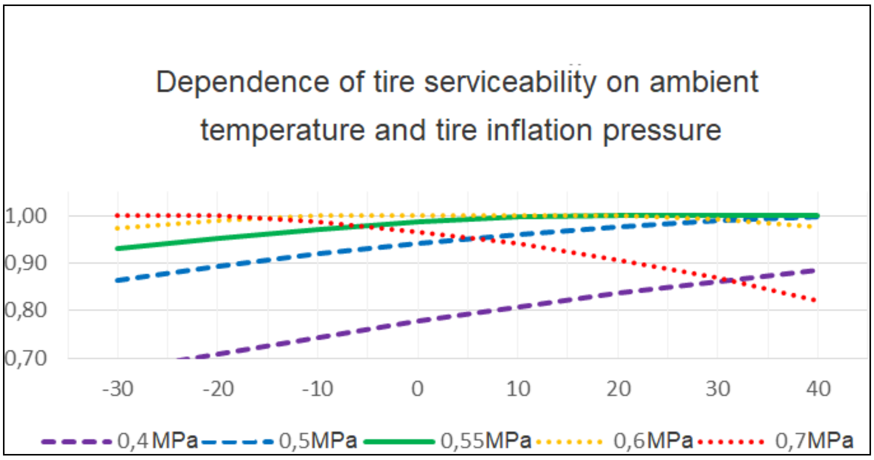

Fig. 4. – Dependence of tire runability on inflation pressure and ambient temperature for BelAZ 75130 (at inflation temperature of 15 degrees)

As the ambient temperature rises, tire wear decreases for tires with pressures below the rated pressure, and increases for tires with pressures above the rated pressure.

Conclusion

The article considers the dependence of ground pressure on tire inflation pressure. The dependences of tire pressure, tire deformation and contact patch length on tire inflation pressure and tire temperature are given. The calculation methodology is offered which allows to determine the ground pressure exerted by a dump truck, and tire wear rate of a dump truck depending on tire inflation pressure and ambient temperature. Results of the work can be applied both at creation of recommendations for choice of operating modes of dump trucks on the grounds with various bearing capacity, and at designing of new dump trucks with multi-supported course.

References

[1] Smirnov G.A. Theories of Wheeled Machinery Motion. - M.: Mashinostroenie, 1990. – 352 p.
[2] Petrusho V.A., Shuklin S.A., Moskovkin V.V. The Rolling Resistance of Automobiles and Autotrains. - M.: Machine Building, 1975. – 223 p.
[3] Knoroz V.I. Tires of the RS type. – M.: Transport, 1964. - 44 p.
[4] Complex of specialized vehicles for mining / Institute of Mining Engineering of the Ural Branch of the Russian Academy of Sciences (IHD UB RAS), 2009. - 57 p.
[5] Badenkov P.F. Development of Design and Research of Truck Tires of Type P // Pneumatic Tires (Research on the Problem of Improving Quality), 1969. - P.43-81.
[6] Knoroz V.I. Operation of an automobile tire. - M.: Scientific-technical publishing house of the Ministry of Automobile Transport and Highway of the RSFSR, 160. - 299 p.
[7] Short Automobile Handbook / A.N. Ponizovkin, Yu.M. Vlasco, M.B. Lyalikov et al. – M.: FSH Transconsulting, NIIAT, 1994. - 779 p.
[8] Larin V.V. Vertical deformation dependencies of pneumatic tires. Engineering Journal: Science and Innovations, 2013, issue 12. – P. 23 – 26.
[9] Andreescu M.S., Stan S., Influence of tire pressure on brake and suspension diagnostic results //11th International Conference "Interdisciplinarity in Engineering, INTER-ENG 2017, October 5-6, 2017, Târgu-Mures, Romania.
[10] Tarasov P.I., Furin V.O., Voroshilov A.G., Lobanov S.V., Nevolin V.M. Structural schemes of caterpillar dump trucks for work on elevated slopes // Mining information and analytical bulletin (scientific and technical journal, 2007, No. 1. - P. - 336 - 343.
[11] https://zen.yandex.ru/media/id/5bec8a96cfec6100aea4cfa7/kitaiskaia-versiia-samosvala-belaz-5c5c7107e5f8e300b15fad84
[12] https://francis-maks.livejournal.com/465123.html
[13] https://tsk.igduran.ru/?page_id=811

Information of the authors

Khoroshavin Sergey Alexandrovich, Candidate of Technical Sciences, Associate Professor, Ural State Mining University
e-mail: horoshavin.s3@gmail.com

Nekrasova Olga Sergeevna, Postgraduate student, Ural State Mining University
e-mail: bormotova.O@m.ursmu.ru

DOI 10.52209/2706-977X_2023_1_29 IRSTI 55.03.14 UDC 621.865

Hydraulic Excavator Bucket Modeling with a Straight Shovel along a Defined Trajectory

Bezkorovainyy P.G.[1], Teliman I.V.[1*], Malybaev N.S.[1], Shestakov V.S.[2]
[1]Abylkas Saginov Karaganda Technical University, Karaganda, Kazakhstan
[2]Ural State Mining University, Ekaterinburg, Russia
*corresponding author

Annotation. With the active development of the mining sector, the share of open pit mining is increasing. It should be noted that the increase in the volume of open-cut mining depends on the volume and methods of excavation works. The main technological equipment performing up to 80% of the total volume of excavation and movement of minerals in open pit operations is hydraulic excavators. Consequently, efficient and highly productive operation of a hydraulic excavator directly affects the efficiency and profitability of mining operations. An important factor of development of mining industry today is to improve the reliability of technological machinery, namely energy efficiency, durability and maintainability of equipment. At the modern stage of development of mining equipment, the use of mine excavators with a hydraulic drive of the working mechanism occupies a wider and wider niche [1].

Keywords: hydraulic excavator, rotary motion, speed, force, working equipment, bucket, hydraulic cylinder, rod, modeling.

Introduction

Hydraulic mining excavators are becoming increasingly common in open-pit mining operations. Usually digging is done by turning the bucket with the appropriate hydraulic cylinder, but sometimes you need to organize work in specific conditions. For example, in order not to use bulldozers, the excavator must ensure scraping the bottom of the ledge, for which the teeth of the bucket must move horizontally. Another specific area where excavators are used is in quarry reclamation work after they have been mined. During reclamation it is necessary to level the sides of the quarry, and the bucket must move along inclined rectilinear trajectories.

When moving along specified trajectories, all hydraulic cylinders work, with the boom and arm hydraulic cylinders providing the main action to move the bucket, while the bucket cylinder only maintains the required angle of inclination of the teeth to the trajectory.

1. Degree of development of the topic

The digging process of the hydraulic excavator is determined by the operation of the hydraulic cylinders of the bucket, arm and boom.

The hydraulic cylinders must be controlled to ensure that the bucket follows the desired path. Computers and special distributors installed for control can set any desired rod speeds.

When digging, it is possible situations in which there will be a part of the caterpillars detachment from the bottom hole soil - the caterpillar together with the platform turns relative to the support rollers, close to the bottom hole. Such movement limits the force on the bucket teeth when digging - the efforts of the hydraulic cylinders rods could provide more force, but the displacement of the working equipment when turning the platform does not allow it.

Tilting moment at digging relative to track rollers of the undercarriage is caused by gravity forces from the side of the working equipment and digging efforts, and the holding moment is an equilibrium of gravity forces of the turntable (without working equipment) and undercarriage.

At present time, there is a technique by which the first version of the working equipment design is developed, taking parameters similar to those of the existing models [2, 3], for it, forces in joints, brackets, boom supports are determined according to the necessary digging forces and then stress calculations are made to check the strength. For the elements that do not provide the strength condition, design changes are made, and the stress calculation is repeated [4,5].

Schematic for obtaining expressions for calculating the speeds of movement of hydraulic cylinders rods is shown in Fig. 1. The line KB shows the required trajectory of the bucket movement, its slope is determined by the angle ψ.. This trajectory will coincide with the tangential component of the digging resistance force P_{01}.

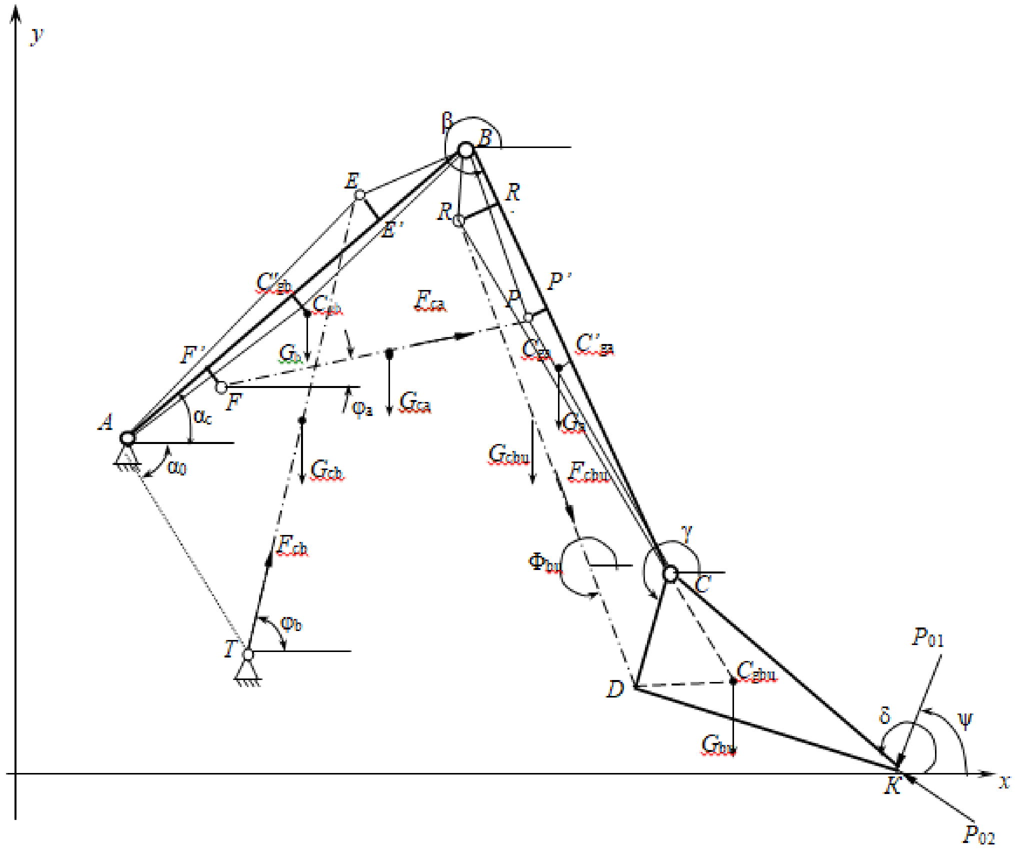

Fig. 1. – Diagram for calculating the parameters of the mathematical model
A, T, E, F, P, R, B, C, D - hinges; K - bucket tooth tip; KSD - bucket profile diagram; CB - arm; AB - boom;
TE, FP, RD - hydraulic cylinders of boom, arm and bucket; G_b, G_a, G_{bu}, G_{cb}, G_{ca}, G_{cbu} - gravity of boom, arm, bucket, hydraulic cylinders of boom, arm, bucket; C_{gb} C_{ga} C_{gbu} - center of gravity of the boom, arm and bucket; α_c, β, γ - horizontal tilt angles of boom, arm, and bucket

According to the presented expressions developed an algorithm and made a program in algorithmic language for research. The output of the results is provided in a table on the graph and in the form of a figure of the calculation scheme on a scale. Calculations for an excavator with a bucket of 6 m3 and a bucket speed of 1 m/s are made. Calculation results in the form of figures and graphs of velocity changes are shown in Fig. 2,3,4.

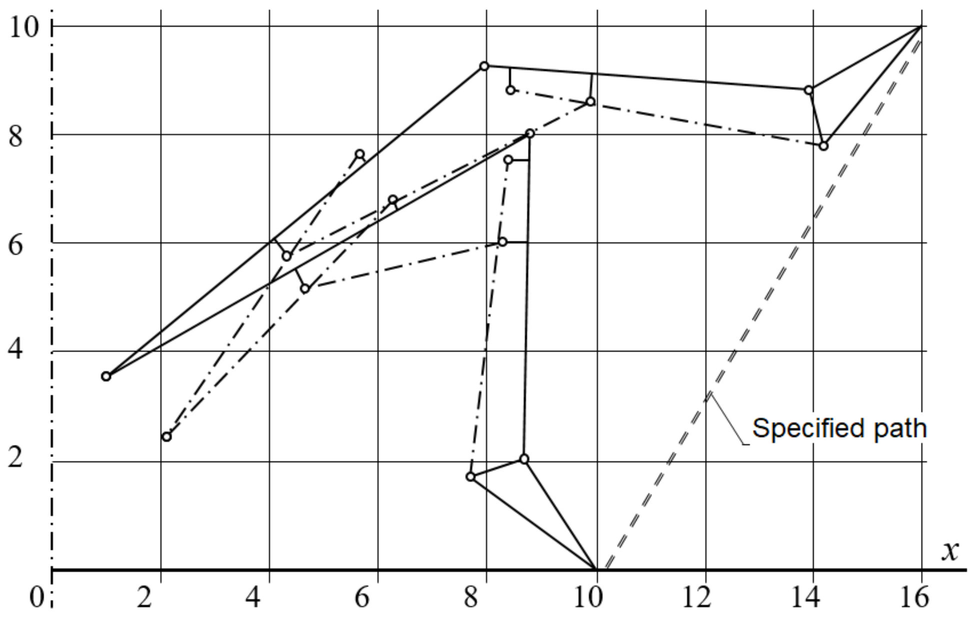

Fig. 2. – Calculation results in the form of a figure (positions of the working equipment at the beginning and at the end of the digging trajectory)

Table 1. Input data of calculation variant 1

Parameter name	Diagram designation	Value
Coordinates of the initial point of the trajectory, m	X_{trn}	7,0
	Y_{trn}	0,0
Trajectory length, m	L_{tr}	6,0
Angle of inclination of the trajectory to the horizontal, deg.	ψ	60,0
Angle between the CK line and the trajectory, deg.	$\angle_{CKB}$	120

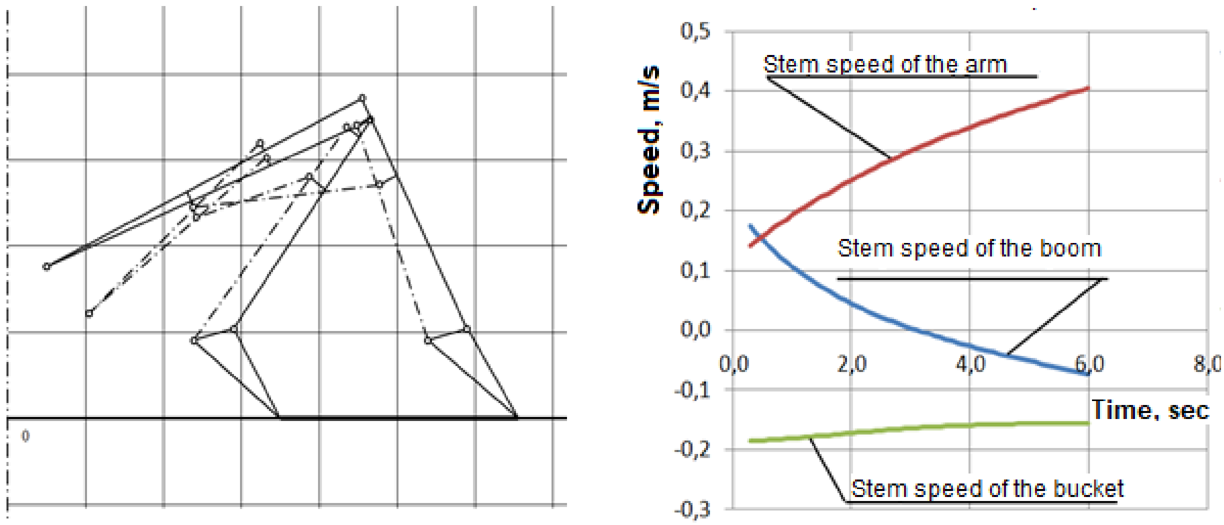

Fig. 3. – Working equipment positions and speed charts

Table 2. Input data of calculation variant 2

Parameter name	Diagram designation	Value
Coordinates of the initial point of the trajectory, m	X_{trn}	12,0
	Y_{trn}	1,0
Trajectory length, m	L_{tr}	8,0
Angle of inclination of the trajectory to the horizontal, deg.	ψ	60,0
Angle between the CK line and the trajectory, deg.	$\angle_{CKB}$	120

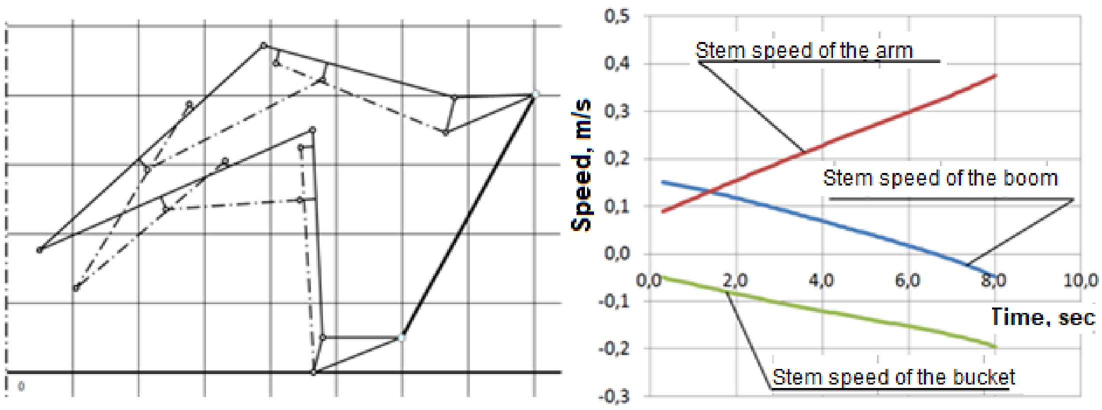

Fig. 4. – Working equipment positions and speed charts

2. Results

When digging in quarries, it is possible when the force from the hydraulic cylinders of the working equipment is transmitted through one tooth of the bucket when meeting the unexploded mass of rock. The most unfavorable case for loading of working equipment is when the force is transmitted to the extreme tooth of the bucket. There is a torque on the bucket, arm and boom from off-center force application. Thus, torsional moments from asymmetric loading of a bucket are added to the acting bending moments from hydraulic cylinder forces that has to be taken into account in calculations of strength and in selection of element sections [6].

The technique of calculation of efforts in elements of the working equipment within the limits of a working zone at uniform loading of all teeth of a ladle is resulted in [7]. According to efforts on hydraulic cylinders rods the mathematical model resulted in a technique provides definition of possible efforts on teeth of the bucket within the working zone.

Schematic for making up a mathematical model when forces are transmitted to the rock mass through one outermost tooth is shown in Fig. 5.

The force on the bucket tooth is determined by the maximum forces on the working equipment hydraulic cylinder rods, and depends on the weights, linear dimensions and coordinates of the working equipment elements position, as well as the position in the face face of the top of the bucket tooth, through which the force is transmitted to the rock [8].

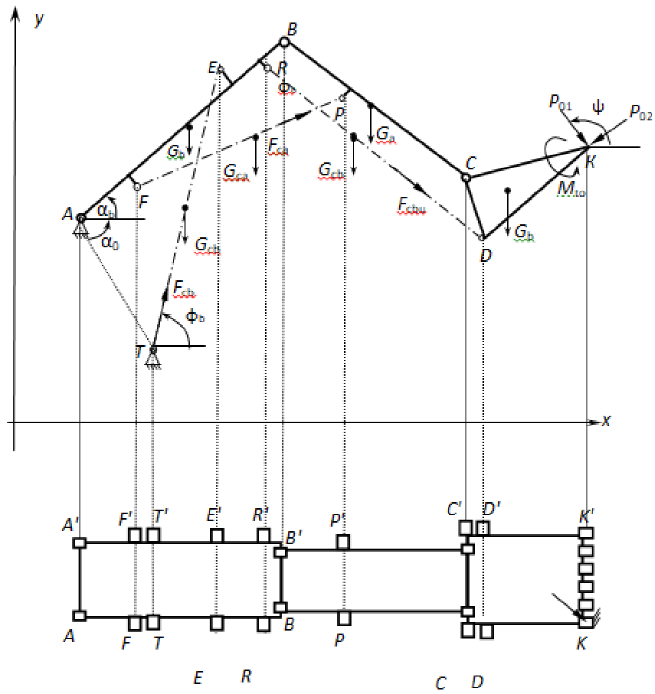

A, T, E, F, P, R, B, C, D - hinges*; K* - bucket tooth tip; *KSD* - bucket profile diagram*; CB* - arm*; AB* - boom*; TE, FP, RD* - hydraulic cylinders of boom, arm and bucket rotation; G_c, G_p, $G_к$, G_{cb}, G_{ca}, G_{cbu} - gravity of boom, arm, bucket, hydraulic cylinders of boom, arm, bucket of boom, arm, bucket; α_c, α_0, φ_b, ψ - edges

Fig. 5. – Work equipment diagram

When digging with one side of the bucket (the outermost tooth), in addition to the forces and reactions specified for digging, there are reactions in the form of a pair of forces on the articulated lugs from the torsion torque.

The torque on the bucket from the digging force P_0 applied to the outermost tooth K:

$$M_{to}=P_0\times KK' \tag{1}$$

where KK' - is bucket width by teeth,

P_0 - digging force, $P_0=(P_{01}^2+P_{02}^2)$

This torque is perceived by a pair of forces in the hinges of the bucket to the CC' arm. Perception of the torque by pairs of hydraulic cylinders can be disregarded in view of sluggishness of joints of hydraulic cylinders in a plane of action of the torque.

Additional reactions in the C-joint from the torque:

$$F_{c.Mto}=M_{to}/CC' \tag{2}$$

Additional from torque reactions in joint B:

$$F_{B.Mto} = M_{to}/BB' \quad (3)$$

Additional from torque reactions in joint A:

$$F_{B.Mto} = M_{to}/BB' \quad (4)$$

Conclusion

For an excavator with a $6m^3$ bucket the results of calculations of digging forces and forces during transportation are obtained, it is revealed that reactions in the boom heel and the handle-boom joint from forces during transportation exceed reactions from digging forces by 5-30 %.

It is set that additional reactions act in a plane parallel to a plane of torque action, reactions at digging mode are defined in a global coordinate system of an excavator, therefore it is necessary to consider such feature at calculation of tensions in elements of the working equipment. The direction of action and decomposition of torque should be taken into account when calculating the lugs.

To calculate the main part of the boom and arm it is necessary to take into account the torque from asymmetric loading of the bucket, bending moment and compressive forces from digging reactions and forces from hydraulic cylinders.

References

[1] Komissarov A. P., Teliman I. V., Experience of using working equipment of hydraulic excavators // Technological equipment for the mining and oil and gas industry: Proceedings of the XVI International Scientific and Technical Conference "Readings in memory of V.R. Kubachek", Ekaterinburg: UGUU, 2018. - P. 121-124.

[2] Lagunova Yu. A., Komissarov A.P., Shestakov V.S. Designing of mining excavators. - M.: Innovative mechanical engineering, 2017. - 228 p.

[3] Komissarov A. P., Lagunova Y. A., Teliman I. V., Shestakov V. S. Methodology of determining the reactive loads in hydraulic excavators // Proceedings of the XXVI International Scientific and Technical Conference in Sevastopol September 23-29, 2019 - Donetsk: DonNTU, 2019. - 500 p.

[4] Ivanov I.Yu., Komissarov A.P., Teliman I.V., Lukashuk O.A. Analysis of lever-hydraulic mechanisms of working equipment of hydraulic excavators // Technological equipment for mining and oil and gas industry. Proceedings of the XV International Scientific and Technical Conference. - Yekaterinburg: Ural State Mining University, 2017. - P. 51-54.

[5] Zykov P.A. The method of optimal choice of the model of a single-bucket hydraulic excavator for the given mining-geological and technical conditions // Mining equipment and electromechanics. - No. 1. - 2014, pp. 37-42.

[6] Babenkov P.Yu., Shestakov V.S. Modeling the working process of a hydraulic excavator // Mining equipment and electromechanics. - No. 1. - 2018, pp. 10-14.

[7] Lukashuk O.A., Komissarov A.P., Lagunova Yu.A. Development of a digital control system for the main drives of a mining excavator as the most important direction for increasing the efficiency of the excavator // IOP Conference Series: Materials Science and Engineering, 709 (2), 2020. paper # 022117, https: // www.scopus.com DOI: 10.1088 / 1757-899X / 709/2/022117

[8] Shestakov V., Bezkorovainyy P., Franz T. Determination of the working area of a hydraulic excavator // E3S Web of Conferences, Volume 177 (2020), Ekaterinburg, Russia, April 2-11, 2020. R. Apakashev, D. Simisinov and A. Glebov (Eds.)

Information of the authors

Bezkorovainyy Pavel Gennadyevich, Senior Lecturer, Abylkas Saginov Karaganda Technical University
e-mail: bpg82_karlion@mail.ru

Teliman Irina Viktorovna, Candidate of Technical Sciences, Senior Lecturer, Abylkas Saginov Karaganda Technical University
e-mail: ir4ik87_telbez@mai.ru

Malybaev Nurlan Sakenovich, Candidate of Technical Sciences, Associate Professor, Abylkas Saginov Karaganda Technical
e-mail: malybaevnurlansakenovich@mail.ru

Shestakov Victor Stepanovich, Candidate of Technical Sciences, Senior Lecturer, Ural State Mining University
e-mail: shestakov.v.s@mail.ru

DOI 10.52209/2706-977X_2023_1_34 IRSTI 53.49.15 UDC 621.9.048.7

Methods for Increasing the Operating Life of Shut-Off Valves of Thermal Power Plants

GavrilovaV.V.*, Musafirova G.Ya.
Yanka Kupala State University of Grodno, Grodno, Republic of Belarus
*corresponding author

Abstract. The influence of various coatings on the corrosion resistance of the valve stem of shut-off valves has been studied. To assess the quality of the obtained coatings, microhardness, corrosion resistance, deformation-strength and tribological characteristics were determined. Researches have shown that the most optimal way of anti-corrosion protection for the shut-off valve stem is chromium-plating, which provides corrosion proofing, increases wear resistance and surface microhardness.

Keywords: anti-corrosion protection, shut-off valve, spindle, chromium-plating, chemical oxidation with oiling, zinc-coating, corrosion proofing.

Introduction

Shut-off valves are an integral part of the equipment, it has a certain impact on the level of its reliability. Particularly important are the requirements for strength, tightness, reliability and durability of the design of shut-off valves. Particularly important are the requirements for strength, tightness, reliability and durability of the design of shut-off valves [1]. The main disadvantage of shut-off valve parts operating [2, 3, 4] in water (steam) mains in heat-stressed conditions is corrosive wear, which limits it's service life [5].

The purpose of this work is to improve the operational characteristics of shut-off valves and extend the overhaul life. In this work, the influence of various coatings on the corrosion proofing and mechanical characteristics of shutoff valve parts was studied.

1. Methods of research

As an object of study, the element of the shut-off valves most susceptible to corrosion was chosen, designed to turn on or off the flow of the medium (water) in the pipelines of thermal power plants. This element is a spindle made of steel 40X GOST 4543-71.

For testing, samples were made of steel 40Kh with subsequent heat treatment according to the regime: volumetric hardening at 850 ° C and tempering at 500 ° C, to ensure the requirements of the design documentation for the spindle hardness (42 - 45 HRC). Chrome plating, chemical oxidation with oiling, zinc-coating with chromium-plating (hereinafter zinc-coating) [2]. A general view of the fabricated samples is shown in Fig. 1.

a) b) c) d)

a – uncoated; b – chromium (Cr); c – zinc (Zn); d – chemical oxidation with oiling

Fig. 1 - General view of test specimens

Determination of the corrosion resistance of the studied coatings was carried out in accordance with the current standard GOST 9.308-85 [6]. The essence of the method, to determine the corrosion resistance, was to accelerate the corrosion process by increasing the ambient temperature and introducing a solution of sodium chloride into the atmosphere. To carry out the tests, an MS-71 climatic chamber was used, designed to create heat and salt fog with a dispersion of 1–10 μm (95% drops) and a water content of 2–3 g/m3. The volume of the chamber is not less than 0.4 m3, with automatic temperature maintenance. The tests were carried out at a temperature of 35 °C and a duration of 152 hours.

To determine the tensile strength of the samples, an IR 50447-50 tensile testing machine with the highest ultimate load of 50 kN was used. The tensile testing machine is designed for tensile testing of specimens made of metals, plastics, rubber and other materials within the technical capabilities of the machine. The strength test was carried out on flat samples with dimensions of 100 × 20 × 3 mm in accordance with GOST 1494-84 (ISO 6892-84) [7].

Tribotechnical tests were carried out on an FT-2 microtribometer designed to study the characteristics of friction and wear of materials, as well as the characteristics of lubricants. The tests were carried out on round specimens Ø 40 × 5 in size. To study the tribotechnical characteristics of the samples, a test scheme was applied with the rotation of three indenters on a fixed disk. Test conditions: n = 60 rpm; t = 2 min; N_{start} = 60 N. The process of tribological tests consisted in bringing the contacting bodies into contact, loading them and setting them in motion relative to each other. During the experiment, the load in the friction pair, the speed of rotation of the main shaft, the friction force arising in the tribocoupling, and the change in the vertical position of the platform with the lower sample were recorded. Determine the total linear wear of a friction pair without taking into account thermal expansion.

To measure the microhardness, a PMT-3 device was used. The PMT-3 microhardness tester is a microscope designed to measure the microhardness [8] of metals, glass, abrasives, ceramics, minerals and other materials. The principle of operation of the device is based on the indentation of a diamond pyramid into the test material under a certain load and measurement of the linear value of the diagonal of the resulting imprint (GOST 10717-75 The microhardness of the samples under study was determined by the method of reconstructed imprint by a tetrahedral pyramid with a square (Vickers base). The reconstructed indentation method consists in applying an indentation to the test sample surface under the action of a static load applied to the diamond tip for a certain time. The value of microhardness was determined by dividing the normal load applied to the diamond tip by the conditional area of the side surface of the resulting imprint.

Microscopic analysis was performed using an MMP 1600T metallographic microscope. Inverse metallographic microscope MMP-1600T is used for observation and analysis of metallurgical products, for inspection and measurement of crystals, integrated circuit, microelectronics in the electronics industry. Microscopic examination can be carried out in a bright field with direct and oblique illumination, in a dark field, in polarized light, by the method of phase contrast and interference.

2. Results about discussion

The results of determining the corrosion resistance of the coatings under study are presented in Fig. 2.

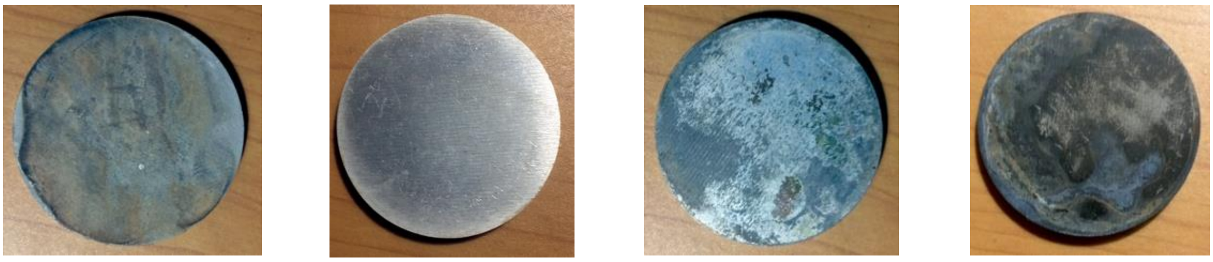

a) b) c) d)

a – uncoated; b– chromium plate (Cr); c – zinc covering (Zn); d – chemical oxidation with oiling

Fig. 2. - Results of corrosion tests

As the test results show, of all the studied samples, the uncoated sample is subject to the greatest corrosion attack, on its surface there is a corrosion damage in the form of irregularly shaped spots, on 70 - 75% of the sample surface. Chrome plating showed the highest resistance to corrosion. On a sample with a zinc covering, localized corrosion is observed, the area of which is 10%. A sample coated in the form of chemical oxidation with oiling is also slightly susceptible to corrosion, the area of corrosion damage is 15%.

The results of deformation-strength tests are presented in Fig.3.

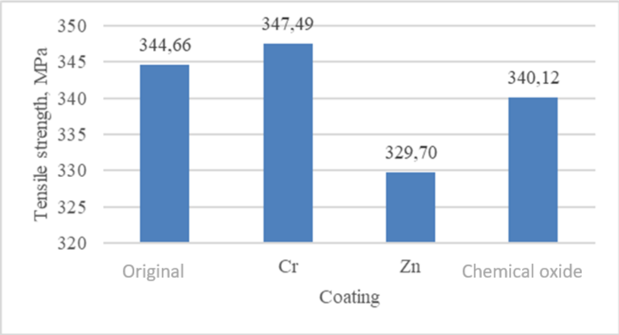

Fig. 3. - Tensile strength indicators depending on
from applied coating

The results of deformation-strength tests showed that the strength of the studied samples changes insignificantly, within 10%, when coatings are applied.

The results of tribotechnical tests are shown in Fig.4.

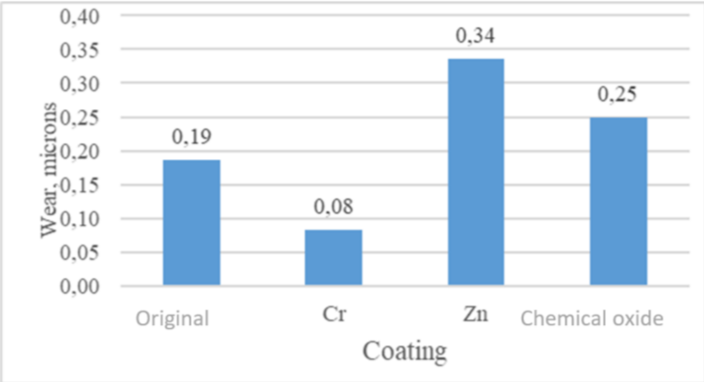

Fig. 4. - Wear of surfaces, test samples
depending on the applied coating

It can be seen from the obtained results that surface wear decreases during chromium plating. When applying Cr, a significant decrease in wear by 2.4 times is observed. When using galvanizing and chemical oxidation, wear increases significantly.

The results of measurements of the microhardness of the surface of the samples are shown in Fig. 5.

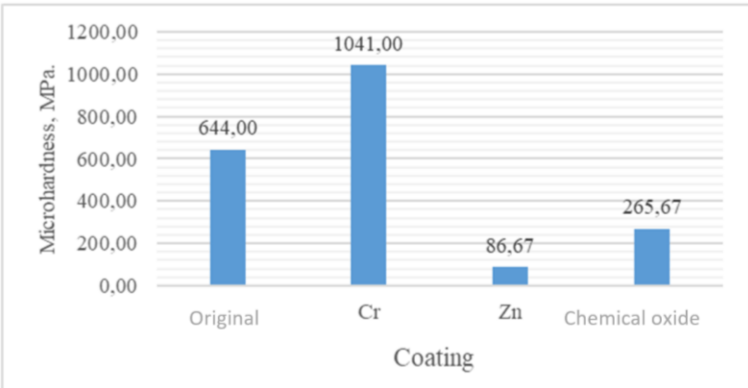

Fig. 5 - The values of the microhardness of the samples in
depending on the applied coating

As a result of the study of the microhardness of the samples, it was found that during chromium plating there is a significant increase in the surface microhardness, more than 60%. With the use of zinc plating, the microhardness of the samples decreased by 87%, and with chemical oxidation, by 60%.

The results of optical microscopy of the samples are shown in Fig. 6.

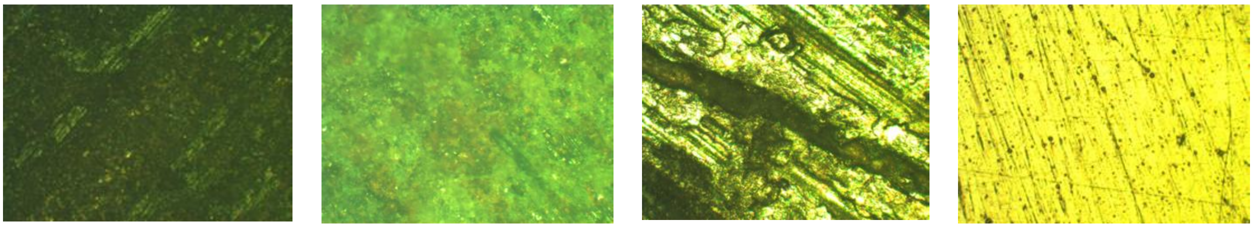

Steel 40X | Steel 40X+ chromium coating | Steel 40X + zinc-coating | Steel 40X + chemical oxidation with oiling

Fig. 6. - Results of optical microscopy of the studied samples, magnification 10×

Microscopic analysis of metallic materials makes it possible to obtain information about the nature of corrosion damage. Various types of corrosion are observed on the obtained images of coated samples. The original sample is subject to continuous uniform corrosion. A more uniform structure is observed on a sample with a chrome coating. Pitting corrosion is visible on sample No.4, and local uneven surface corrosion is visible on sample No.3. The presence of iron-zinc phases was found in the surface structure of the zinc-coated sample.

Conclusions

The results of the conducted research indicate that the most optimal way of anticorrosion protection for the gate valve spindle is surface chromium plating, which provides protection against corrosion. In this case, an increase in wear resistance and microhardness of the surface of the parts is observed.

References

[1] Chernoshtan V.I., Kuznetsov A.A. Pipeline fittings: reference manual. - M.: MPEI, 2001. - 368 p.

[2] Fernandez E.S., M. Rio S., Chalmers H., Khakharia P., Goetheer E.L., Gibbins J., Lucquiaud M. Operational flexibility options in power plants with integrated post-combustion capture //International Journal of Greenhouse Gas Control, Volume 48, Part 2, 2016. - P. 275-289.

[3] Solovey V., Zipunnikov M., Rusanov R. Increasing the manoeuvrability of power units of the thermal power plants due to applying the hydrogen-oxygen systems //Journal of Physics: Energy, Volume 5, Number 1, 2023. – P.014012

[4] Chinyaev I.R., Fominykh A.V., Ilinykh E.A. The Valve is a Shutoff for the Passive Protection Systems of Pipelines //Procedia Engineering 150, 2016. – P. 220 – 224

[5] Fedosova N.L., Rumyantseva, V.E., Rumyantseva, K.E., Balmasov, A.V., Chekunova, M.D. Anti-corrosion protection of metals: methodical manual // Ivanovo: Chemistry, 2009. - 187 p.

[6] GOST 9.308-85 Coatings metal and non-metallic inorganic. Accelerated Corrosion Test Methods

[7] GOST 1494-84 Metals. Tension test methods

[8] Bárnik F., Sága1 M., Štalmach O. Innovation of hardness tester mechanism and its functionality test //MATEC Web of Conferences 244, 2018. – P. 01022

Information of the authors

Gavrilova Valentina Vladimirovna, Senior Lecturer, Yanka Kupala State University of Grodno
e-mail: v.gavrilova@ grsu.by

Musafirova Galina Yaroslavovna, Candidate of Technical Sciences, Associate professor, Yanka Kupala State University of Grodno
e-mail: musafirova_gy@grsu.by

DOI 10.52209/2706-977X_2023_1_38 **IRSTI 55.03.14** **UDC 621.878.2**

Investigation of the Processes Occurring During the Operation of the Torque Converter Hub in the Belarusian Autoworks Gearbox during CAE Modeling

Nikonova T.Yu.[*], Essyunin A.I., Zhakupova Sh.S., Dandybaev E.S., Zhukova A.V.
Karaganda Technical University, Karaganda, Kazakhstan
*corresponding author

Abstract. The main objective of the study is to identify and eliminate the causes of breakdowns in the torque converter hubs of mining dump trucks Belarusian Autoworks. The relevance of the work carried out: during the operation of dump trucks based on Belarusian Autoworks vehicles, in open pit conditions, according to enterprises operating such equipment, in the period from 2019 to 2021, 75% of the failures and breakdowns of equipment occurred due to the fact that the hub of the torque converter impeller is intensively loaded a part, which during its operation is affected not only by mechanical loads, but also by temperature and others leading to the failure of the specified unit in 85% of cases. For example, hydrodynamic forces that arise during the period of immersion of gear teeth in an oil bath, and so on. Therefore, it is proposed to conduct a comprehensive study of the processes occurring with the wheel hub and identify the main loaded places. Taking into account the analysis carried out, it is possible to produce a batch of wheel hubs with updated parameters and conduct their full-scale tests.

The novelty of the work carried out lies in the analysis of the operating conditions of the hub, which revealed a high boundary pressure that occurs at the point of transition from the air to the oil bath.

The object of research is the study of the processes that occur during the operation of the torque converter hub, which affect the structure and occur in the hub itself.

Research objectives:

- learn the ways and methods of conducting CAE analysis;
- analyze the design parameters of the installation that occur in the torque converter bushing.

Research methods: When performing the dissertation work, methods of physical and mathematical modeling and system analysis of information, laboratory, bench and operational tests using computer and high-precision measuring equipment were used.

Keywords: CAE modeling, torque converter hub, hydromechanical transmission box.

Introduction

Engineering analysis of the transformer hub is an urgent engineering task in the conditions of the Maker LLP enterprise. Under the conditions of the enterprise, manufacturing is carried out from SKD parts supplied from the territory of the Republic of Belarus and repair and restoration of worn components and parts. During the operation of the enterprise, for the period from 2017 to 2019, at the enterprise of 9 BelAZ-75135 dump trucks with a carrying capacity of 110 tons, as well as 4 BelAZ-7513 dump trucks with a carrying capacity of 130 tons, the main most worn parts were torque converters in hydromechanical transmission (Fig.1.).

Fig.1. - Hydromechanical gearbox of BelAZ dump truck

It should be noted that the equipment, and most importantly for this work, the torque converter units, were designed to work on specially equipped roads, with a maximum length of 6-8 km at a rise of 5-8%, with a turnaround time of at least 170,000 km. However, the technique didn't work in some cases even 50,000 km.

In the hydromechanical transmission, a complex, single-stage, lockable, four-wheel torque converter is used. At high loads, it increases the torque transmitted from the engine, and at low loads it transmits it without change, i.e. operates in hydraulic mode.

The most worn part of a hydromechanical gearbox is the torque converter hub. In all cars that came for repairs in the period from 2019 to 2021, the hub (Fig.2.) was, in 4 cases, broken into two or more parts, in other cases it was worn out to over critical values.

The torque converter hub is attached to the crankcase and is a distributor of oil supplied to engage the friction clutches of the gearbox and block the torque converter, as well as to the torque converter cavity and to the lubrication line for lubricating the friction clutch disks and bearings.

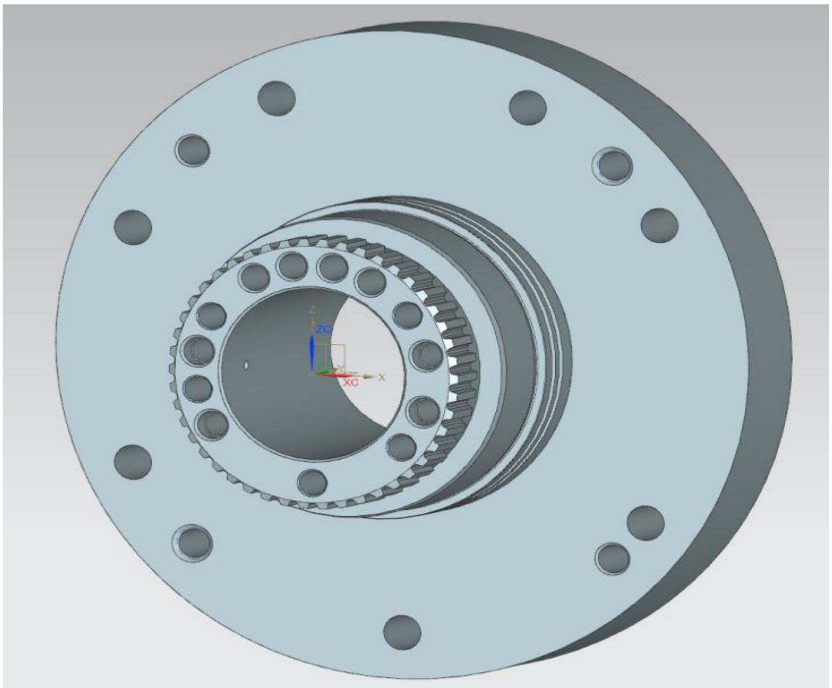

Fig. 2. - Hub of the torque converter

During the analysis of the causes of breakdowns of the torque converter hub, there are: wear and destruction of the working surfaces of the wedge-shaped grooves, support hub and DOA rollers; destruction of the blade system, filling with wear products of the working cavity and channels for pumping the working fluid.

Failure leads either to the exclusion of the possibility of timely locking of the reactor wheels, or to jamming of the DOA rollers and complete blocking of the reactor wheels.

It is possible to diagnose the loss of the ability to jam the DOA of the second reactor in the dump truck acceleration mode, which significantly increases the acceleration time to a given speed, and reduces the distance traveled during this time. If the DOA of any reactor turns out to be not wedged during the acceleration of the dump truck at high values of the so-called gear ratio, then this malfunction can be detected by excessively rapid heating of the working fluid at the outlet of the gas turbine engine, since its efficiency will begin to decrease sharply.

To study the above problem, it is necessary to analyze the main factors affecting the torque converter bushing, as well as find out how these effects affect the ability to carry out their direct technical functions. To carry out such an analysis, it is possible to conduct full-scale tests, which, however, require large labor and economic costs and take long time intervals. And the second method of analysis, using CAE technology, and specifically the ANSYS software package [1].

1. Analysis of the operation of the design of the torque converter hub

During the analysis of the design of the torque converter hub, data were obtained on defective machines, the reasons for their failure, and the main defects were studied.

So, for example, from January 2019 to December 2021, 37 Belarusian Autoworks cars were out of action, the main reason for failure in 30 cars is a breakdown of the torque converter hub or a complete failure of the torque converter. So, compared with machines manufactured at enterprises in other countries, the number of exits for a similar reason is presented in Table 1.

Table 1. Statistical data on the failure of cars of the Belarusian Autoworks brand manufactured in the territory of the Republic of Kazakhstan and the Republic of Belarus

Car model	Place of manufacture	Year made	The number of cars in total working in the quarries of the region	Causes of failure of equipment for the period from 2017-2019			Total number of failures
				Fuel equipment failure	Failure of body lifting mechanisms	Failure of the hydraulic transmission mechanism	
BELAZ 7555	Republic of Belarus. City of Zhodino; Belarusian Automobile Plant	2017	12	1	3	1	5
BELAZ 7555	The Republic of Kazakhstan. Karaganda city, KLMZ plant	2017	15	14	7	39	60
BELAZ 7557	The Republic of Kazakhstan. Karaganda city, KLMZ plant	2018	5	1	5	24	30
BELAZ 7513	Republic of Belarus. City of Zhodino; Belarusian Automobile Plant	2018	3	1	1	0	2

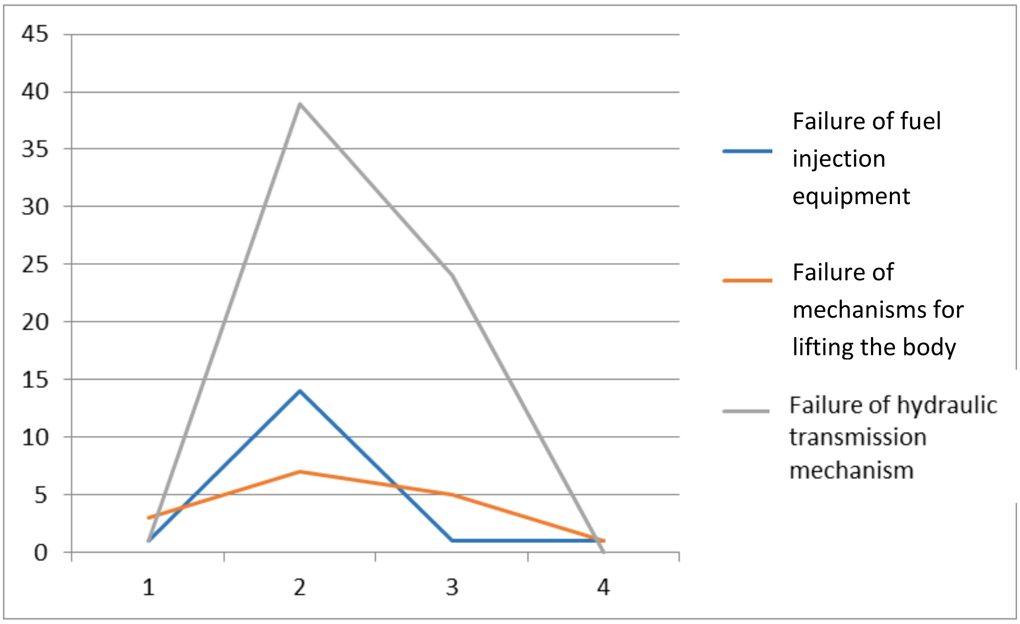

Pic. 3. - The main reason for the failure of Belarusian Autoworks cars

As can be seen from the presented statistical data, the main reason for the failure of cars is the failure of an automatic transmission, and a similar problem is observed only in cars manufactured under license at the KLMZ plant in the Republic of Belarus.

Also, all defective products were studied (Fig. 4-6.).

Fig. 4. - Defective torque converter hub

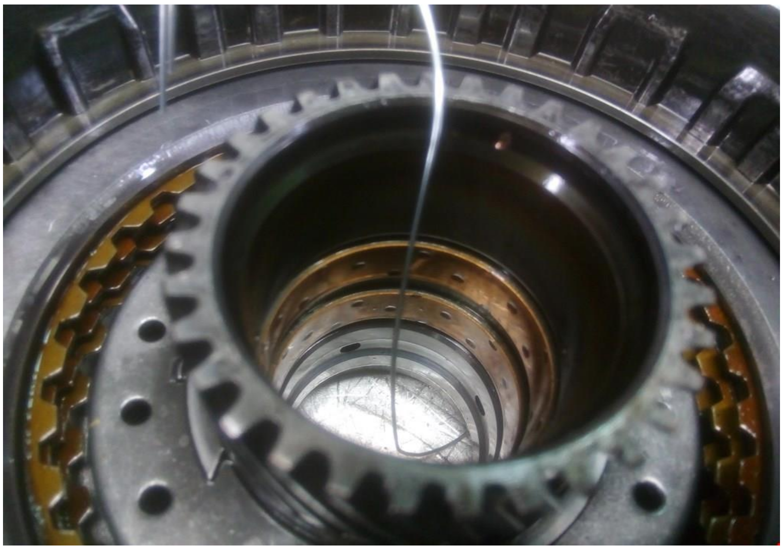

Fig. 5. - Torque converter hub assembly

Fig. 6. - Torque converter hub of Belarusian Autoworks car with signs of wear

The presented materials show that the main place for the development of an automatic transmission breakdown is the torque converter shaft hub.

Thus, in order to work out and determine the main causes of wear, it is necessary to carry out mathematical modeling.

2. Analysis of the mathematical model of the torque converter design

The 3D model of the torque converter impeller hub is divided into elements that will correspond to all geometric characteristics. For these elements, the physical and mechanical characteristics of the materials that make up the hubs are set. After that, boundary conditions and external influence on the model are set. To set such a module of restrictions, it is necessary to enter into the software package a number of mathematical dependencies that describe the relationship of physical processes occurring during the operation of the hub. The second most important event is the search for input parameters that will allow you to determine and set the initial and final conditions of work. Similar work should be carried out for each element where a different computational grid is used [2].

During the work on the model, it was confirmed that all the main dimensions of the hub were taken on the basis of the design calculation of the entire assembly.

After determining all the boundary conditions, it is necessary to set the parameters of the solver. For example, if you set the iteration parameter to 40, the solutions will match field tests 60% of the time. This parameter allows you to assess the reliability of the studies. For the first preliminary calculation, this parameter can be set much less, since the analysis is carried out on a structure that is in operation and has a margin of safety and durability, confirmed by full-scale tests and work in real conditions [3].

To carry out the design analysis procedure, it is necessary to determine with what maximum pressure the torque converter impeller hub supplies oil through the oil lines to the torque converter overrunning wheel. Determining the pressure, as well as the angular velocity and the forces developed at the same time, will be a test of the operability of the structure as a whole, it will allow you to track changes in these parameters by changing both the manufacturing technology of the hub and making changes to the design of the part itself.

Let us give a brief algorithm for creating a model in the Ansys system by transferring the main geometry from the NX software package (Fig. 7.).

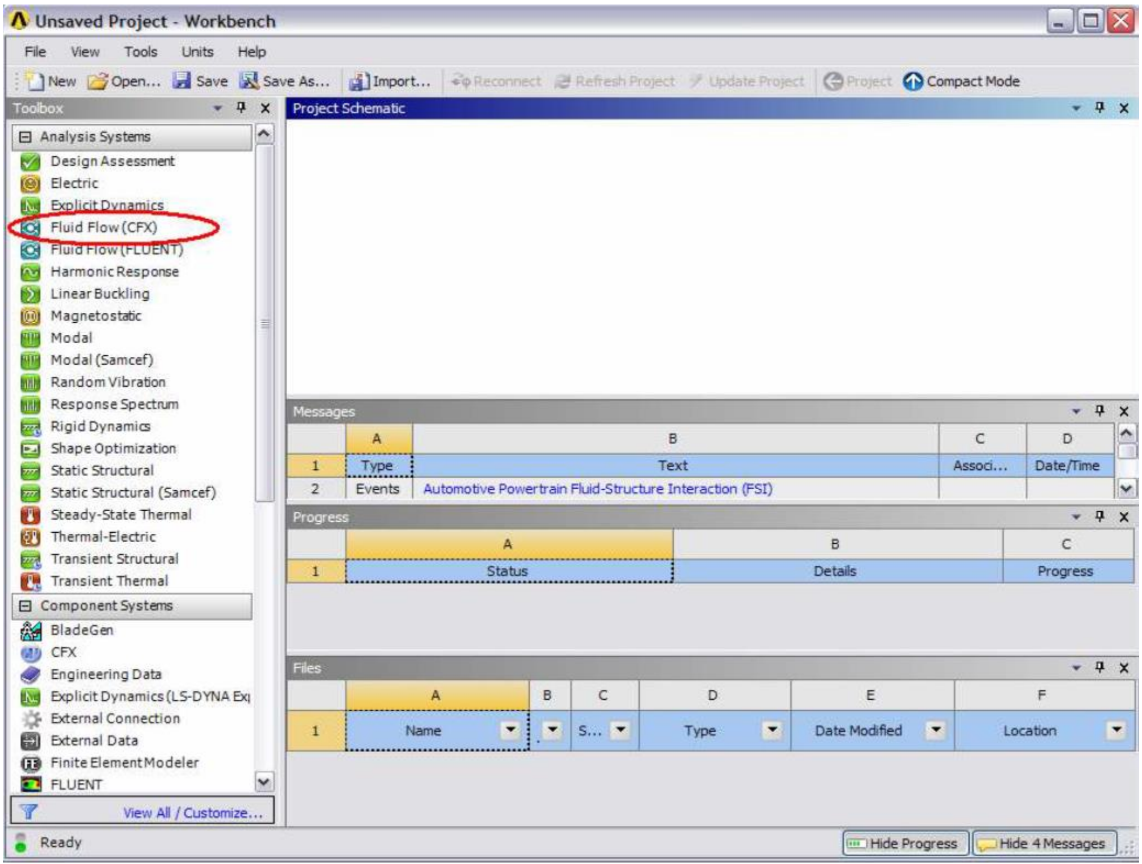

Fig. 7. - Dialog box for creating a new study of basic design parameters

During the transfer of the finished geometry of the hub, it is necessary to dwell on a number of basic requirements, without which the studies will have significant errors. The first significant feature of working in the Ansys software package is the use of units of measurement in feet and inches by default (Fig.8.). And the second feature of the portable model is the variable diameter of the oil lines in the hub housing.

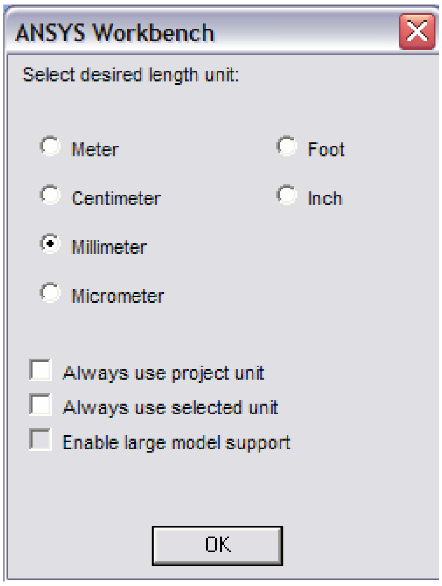

Fig. 8. - Dialog box for selecting the project calculation system

Details of Bend4	
Bend	Bend4
Base Plane	XYPlane
Operation	Add Frozen
Origin Definition	Coordinates
FD3, Origin X Coordinate	0 mm
FD4, Origin Y Coordinate	0 mm
FD5, Origin Z Coordinate	10,75 mm
Axis Definition	Components
FD6, Axis X Component	0
FD7, Axis Y Component	0
FD8, Axis Z Component	1
Base Definition	Components
FD9, Base X Component	0
FD10, Base Y Component	1
FD11, Base Z Component	0
FD12, Angle (>0)	360 °
FD15, Radius (>0)	89,2 mm
FD13, Base Length (>0)	20 mm
FD14, Base Width (>0)	16 mm
As Thin/Surface?	No

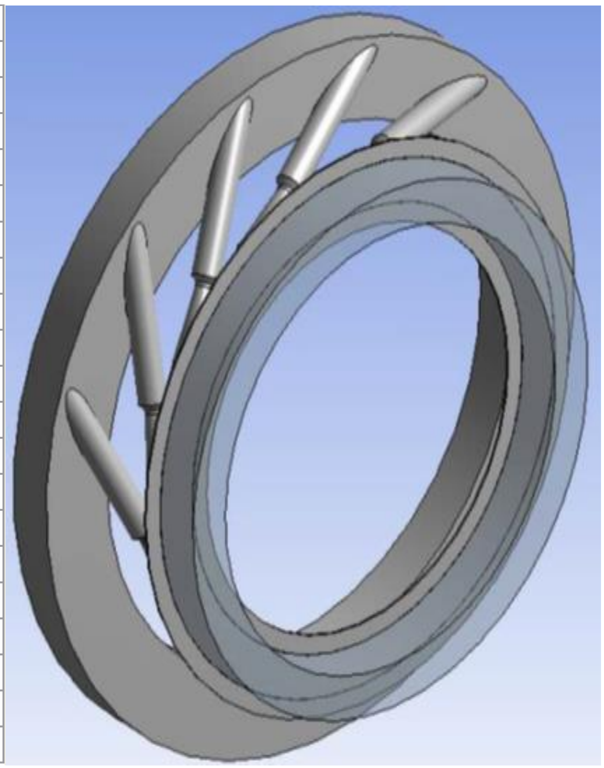

Fig. 9. - General geometrical parameters of oil pipelines in the body of the hub of the torque converter impeller

To conduct a study of the main parameters of the structure, as mentioned above, it is necessary to split the entire geometry into a grid of control volumes. Taking into account the fact that all the main elements of the structure must be broken with the most efficient step [4].

All operations for dividing into control grids are typical sequences of actions. For example, to create a mesh on the rear working surface of the torque converter impeller hub, it is necessary to create the boundary faces of this surface and set their sequence (Fig.10.).

For the convenience of selecting the desired surfaces, it is necessary to use the possibility of partially canceling the display of the structure, since the choice of incorrect parameters often entails an incorrect calculation.

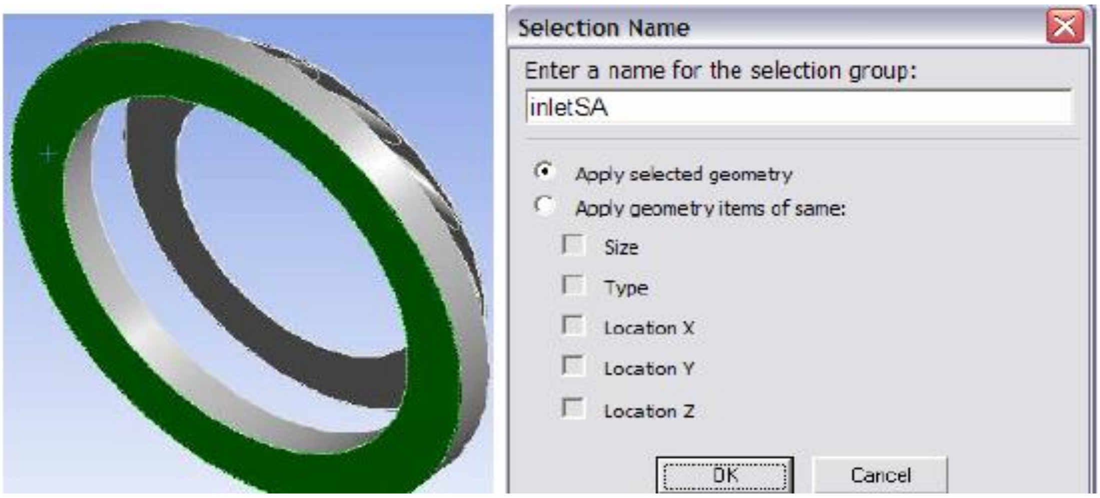

Fig. 10. - Selection of initial and boundary surfaces

Since the finite element method is based on the method of mathematical matrices [5]. That is, the entire surface of the body that is being considered is divided into a large number of polygons, each of which can be described by the equations of physics, mathematics in partial derivatives, then it is necessary to set the boundary conditions and actions of mathematical operators (Fig. 11.).

Inflation	
Use Automatic Inflation	Program Controlled
Inflation Option	Smooth Transition
Transition Ratio	0,272
Maximum Layers	5
Growth Rate	1,2
Inflation Algorithm	Pre
View Advanced Options	No

Sizing	
Use Advanced Size Function	On: Curvature
Relevance Center	Medium
Initial Size Seed	Active Assembly
Smoothing	Medium
Transition	Slow
Span Angle Center	Fine
Curvature Normal Angle	Default (18,0 °)
Min Size	Default (9,3225e-005 m)
Max Face Size	Default (9,3225e-003 m)
Max Size	Default (1,8645e-002 m)
Growth Rate	Default (1,20)
Minimum Edge Length	1,3263e-003 m

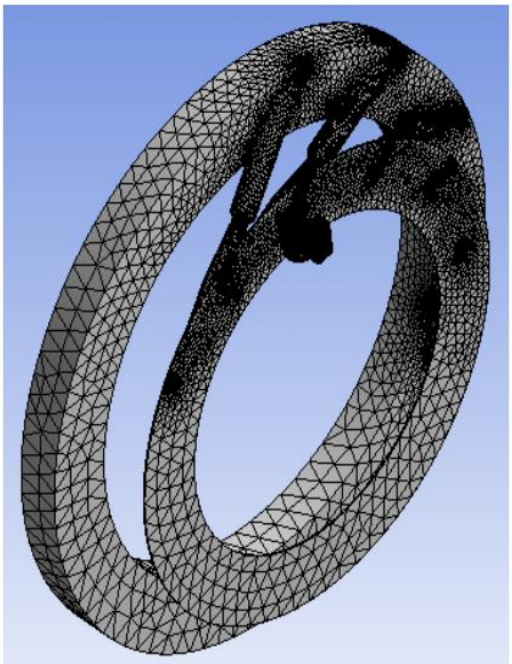

Fig. 11. - Setting basic grid parameters

After carrying out similar procedures with all elements of the torque converter impeller hub, it is necessary to conduct a visual analysis of the structure for uniformity of filling the entire surface of the structure with mesh elements (Fig. 12.).

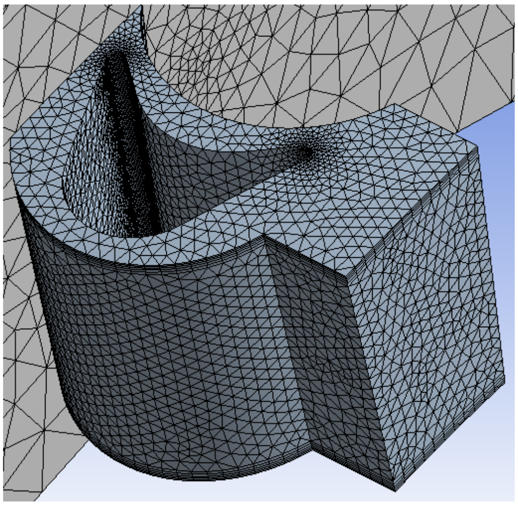

Fig. 12. - Visual analysis of the uniformity of filling the surface of the structure with a mesh

To conduct a full-fledged study of the influence of the main structural parts and methods of manufacturing a hub, it is necessary to simulate the process of operation of this product.

To conduct such a study, we will create a calculation model in which we will lay down the main boundary conditions for the operation of the torque converter impeller hub (Table 2) and configure the program solver module.

Table 2. Boundary conditions for torque converter hub parameters

Parameter designation	Units of measurement of the parameter	Numeric values
Maximum developed power at the hub	kW	50
Maximum angular speed of rotation of the hub	s^{-1}	3394
Oil flow through hub oil lines	kg/s	97,8
Oil pressure at the outlet of the oil pipelines of the hub	kPa	300
Oil pressure at the inlet to the oil pipelines of the hub	kPa	200

Based on the description of the design of the entire unit, it should be noted that in the cavity where the hub of the impeller of the torque converter is located, there is a small amount of air and atomized oil, therefore, it is necessary to take into account the influence of these conditions, for this we will make changes to the environmental conditions subprocessor (Fig.13,14).

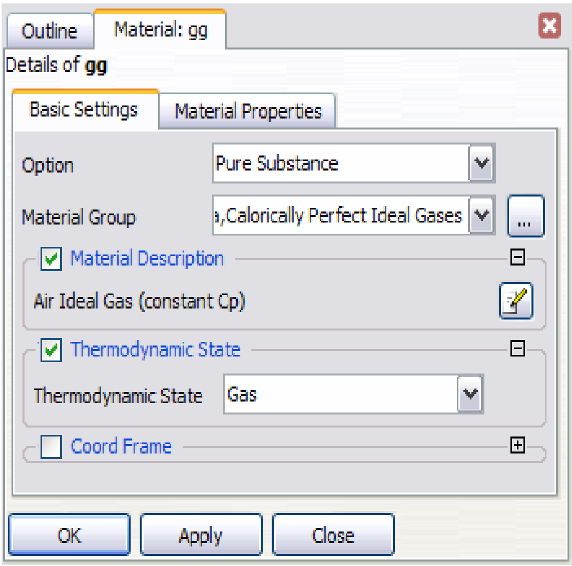

Fig. 13. - Menu for making changes to the environment parameters during the experiment

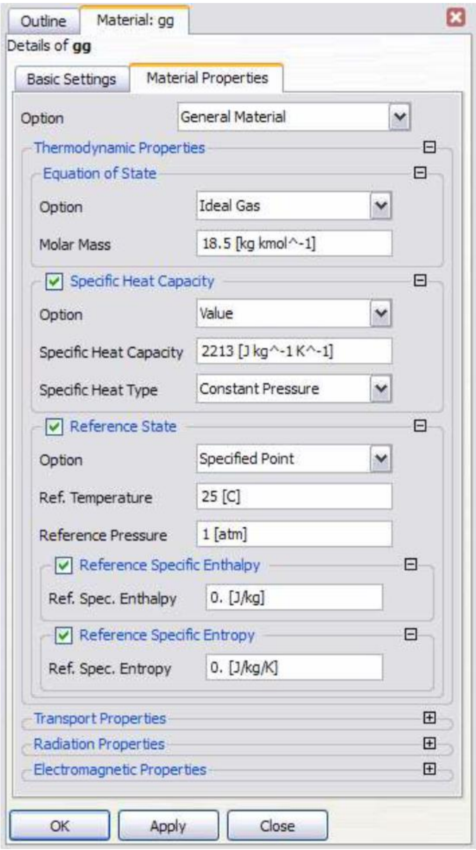

Fig. 14. - Changes made to the environment parameters

The next stage in the creation of the calculation model is the process of determining the zone of action of the given conditions. That is, the approximate dimensions of the cavity where the impeller hub is installed are set, the temperature at the beginning and at the end of the cycle, ambient pressure, humidity, contact boundaries of various media are set. Conditions are set for the maximum and minimum flow rate of the working fluid through the oil pipelines, temperatures in different sections.

Next, a calculation zone is created in which the specified conditions will be created (Fig. 15.).

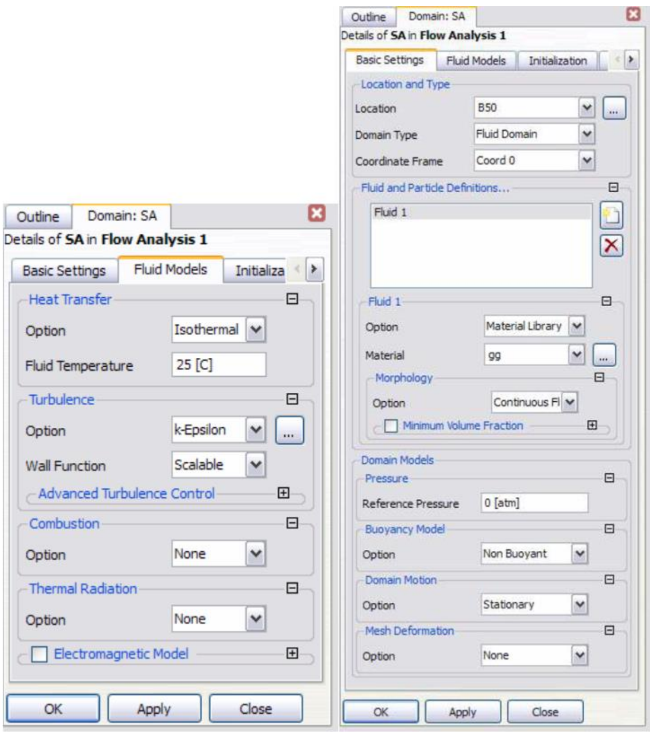

Fig. 15. - The main parameters of the environment during the experiment

After determining all the boundary conditions, it is necessary to set the parameters of the solver. For example, if you set the iteration parameter to 40, the solutions will correspond to field tests in 60% of cases (Fig. 16). The indicated parameter - iteration, allows us to evaluate the reliability of the studies, however, for the first preliminary calculation, this parameter can be set much less, since the analysis is carried out on a structure that is in operation and has a margin of safety and durability confirmed by full-scale tests and work in real conditions.

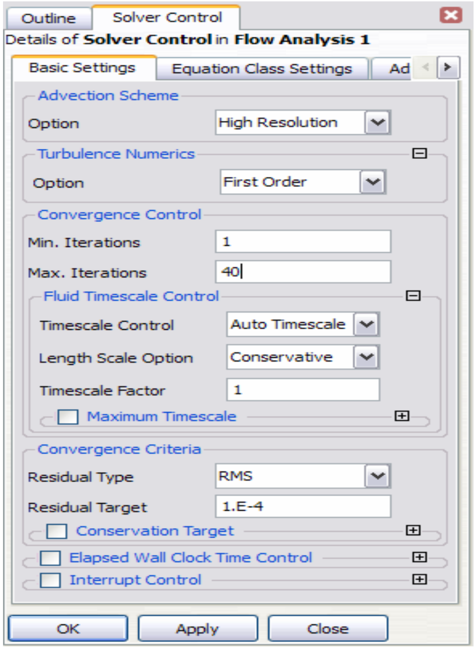

Fig. 16. - The result of the boundary conditions and specifying the degree of accuracy of the solver

As mentioned earlier, in order to find and develop all possible design parameters, the most complete 3D model of the torque converter hub design is required. As it became known, in the course of working on the model, all the main dimensions of the hub were designed on the basis of the design calculation of the entire assembly (Fig. 17.). The torque converter model was made in the NX software package [5].

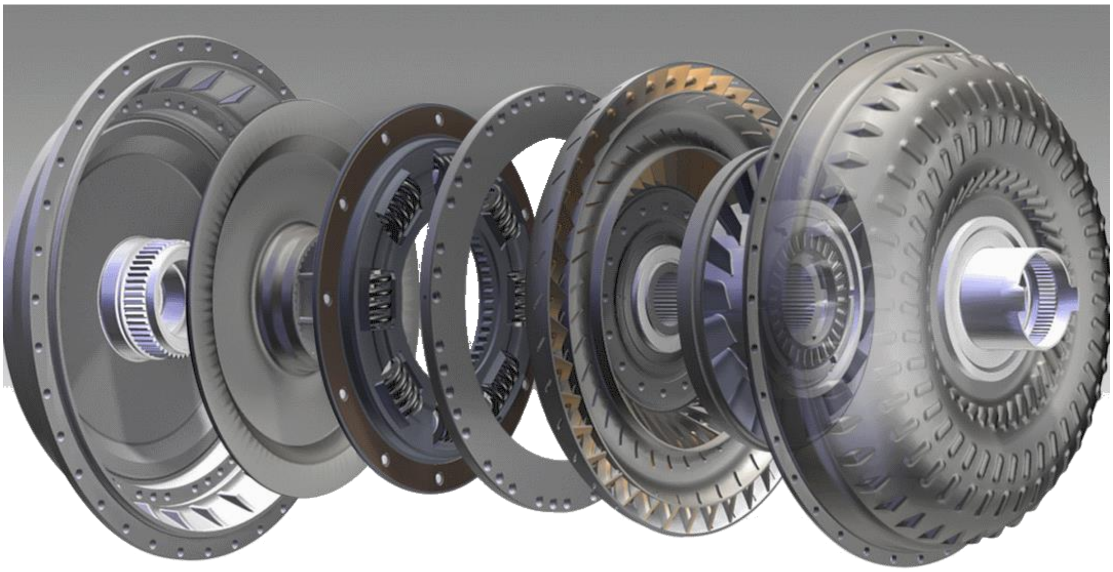

Fig. 17. - Model of the torque converter of the car Belarusian Autoworks

After building a complete model of the analyzed node, simulations of the node operation process were carried out. However, due to the high complexity of conducting this kind of research, the moments of interaction between the turbine wheel structure and the hydraulic fluid were analyzed (Fig. 18.).

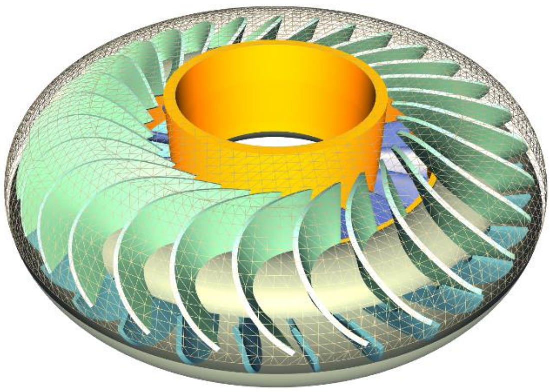

Fig. 18. - Model of a working hydraulic transformer of the Belarusian Autoworks car made in Ansys

Also, to ensure the accuracy of the unit, all the main units were made, the influence of which on the operation of the torque converter is taken into account in the work (Fig. 19.).

Also, during the construction of the model, factors such as the influence of the ambient temperature during the operation of the mechanism, the operating time, and the type of working fluid were taken into account.

It is worth noting the fact that due to the imposition of certain conditions on the calculation in the ANSYS system [6], namely the increase in the time of the calculations, for example, when using the full-fledged model shown in picture 7, the calculation time increased to 2 months and 7 days of computer time. Such calculation terms are not acceptable for real production. Thus, some of the mating parts were replaced by boundary conditions, taking into account the parameters below (Table 3).

Table 3. Main geometric parameters of the hub

Parameter designation	Value
The maximum diameter of the hub, mm	180,23
Maximum diameter of the oil channel, mm	13,1
Minimum diameter of the oil channel, mm	10,98
Degree of partiality	0,42
Number of oil channels	8
Hub lattice pitch, mm	9,78
Number of rotor blades	67

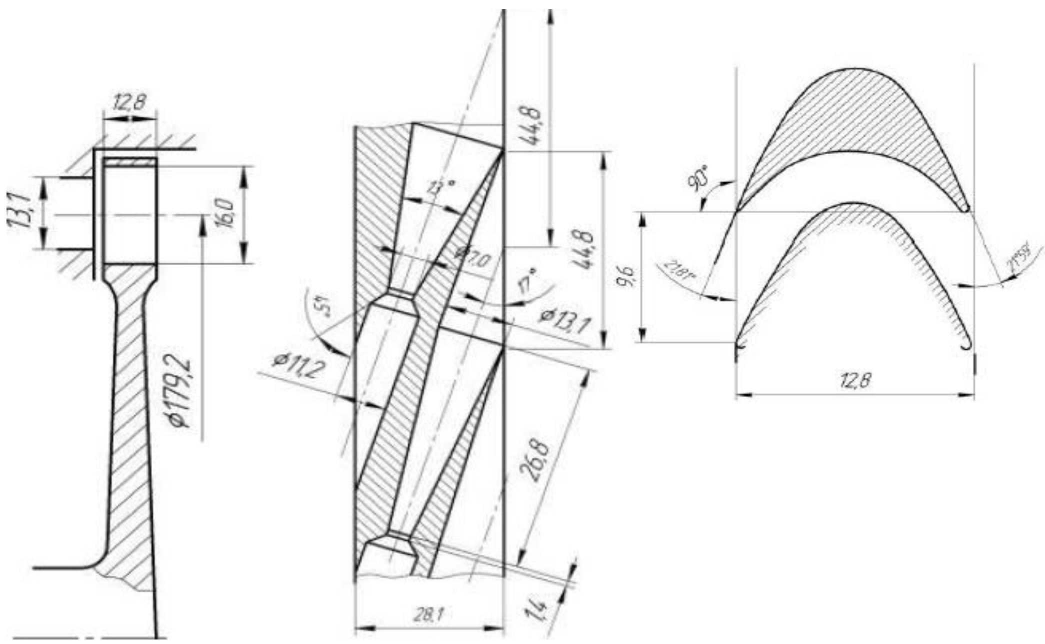

Fig. 19. - Main parameters and geometric dimensions of the most loaded parts of the torque converter impeller hub

Thus, in order to determine some parameters of the boundary conditions, it is necessary to conduct separate studies, for example, calculations were made for the blade blade of the turbine wheel of the torque converter, since when studying full-scale samples, at the manufacturer's plant, traces of cavitation resolution and the appearance of a network of cracks. However, the operating conditions of the unit as a whole cannot be the cause of such a defect; also, when studying the design documentation at the manufacturer, data were obtained that the replacement of the recommended structural material was not carried out. Thus, the study of the phenomena occurring in the process is also necessary (Fig. 20.).

Fig. 20. - Volumetric model of a turbine wheel blade

Conclusion

According to the results of the calculation carried out in the program, taking into account all possible related factors, a picture of the stress distribution in the body of the blade was obtained (Fig. 21.).

The marked impact zones are in excellent agreement with the parameters collected during field observations [6].

On the mathematical model, the zone of maximum loads is visible at the root of the turbine wheel blade, and a regularity was found in the analysis of factory drawings. In turbine wheels assembled by welding the turbine wheel blades with the wheel itself and the hub and the hub assembled by milling with a CNC machine, in 85% of cases the destruction of the impeller hub began in the welding zones.

Confirmation of the received data can be seen in Fig. 21.

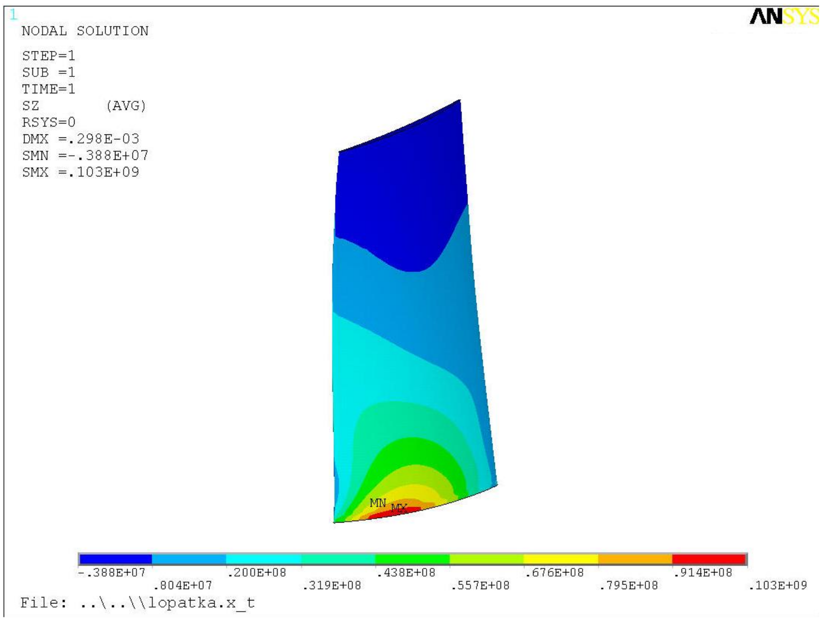

Fig. 21. - Voltage in the turbine wheel blade when the torque converter hub reaches operating speed

Another factor necessary to study the operation of the torque converter hub is to study the process of pumping fluid in the cavities of the hub itself and the effect of the outgoing fluid velocity on the development of cracks in the hub itself. So, compared with the design made on a CNC machine, the dimensions, quantity and quality of these holes are very different from those in the torque converter hubs made at the KLMZ plant.

To study the influence of these parameters, the hub model was analyzed at speeds and operating modes of the corresponding performance characteristic.

So, it turned out that the quality of the holes obtained at the KLMZ plant differs from those obtained on a solid workpiece (Fig. 22.).

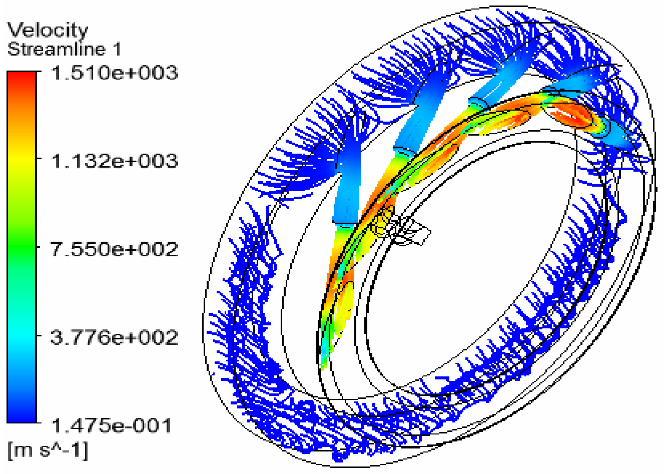

Fig. 22. - Speed parameter calculation results

As can be seen from Fig. 22, fluid inlets into the openings of the torque converter hub are stress and cavitation disturbance concentrators (marked with yellow and red colors). For example, when liquid enters the hole, there is a sharp narrowing of the hole, which is obtained due to the manufacturing technology of the hub, in which the pressure rises abruptly, thereby causing cavitation phenomena and high vibration zones.

And given the previous information, namely that the blades of the turbine wheel are welded, and not made by obtaining from a solid billet. And the turbine wheel, in turn, is fastened to the torque converter hub by means of landing, and is not made in one piece, hot deformation zones are formed [7].

To test the hypothesis, an analysis was carried out of the torque converter hub made from a solid billet.

The analysis showed a decrease in the zones of cavitation impact and displacement of the cavitation zone from the walls of the holes to the zone of the middle flow of liquid penetrating into the hole, thereby protecting the metal (Fig.23.).

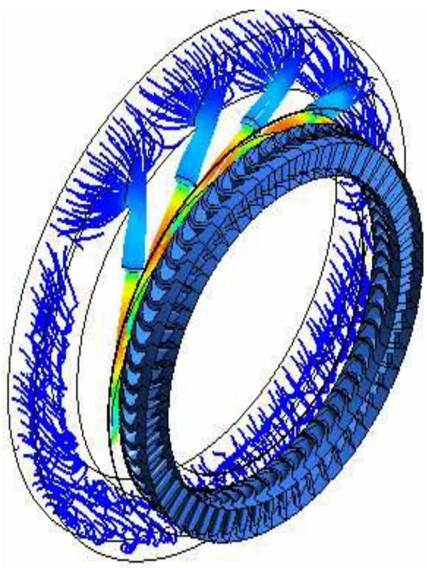

Fig. 23. - Analysis of the design of the torque converter hub made from a whole billet

Thus, various parameters of the torque converter operation were analyzed and the performance characteristics were obtained, as well as the internal frequencies at which the vibration of the main parts of the mechanism occurs (Fig. 25).

In Fig. 11, yellow indicates the natural frequencies of the torque converter hub made from a solid workpiece, and in other colors, the internal frequencies of the component parts of the workpiece hub, made at the KLMZ plant, and in red the resulting oscillations of the product as a whole.

Also, during the process of obtaining a solution, data were obtained on the maximum speed of the hub, the pressure developed in the oil lines (Fig. 24).

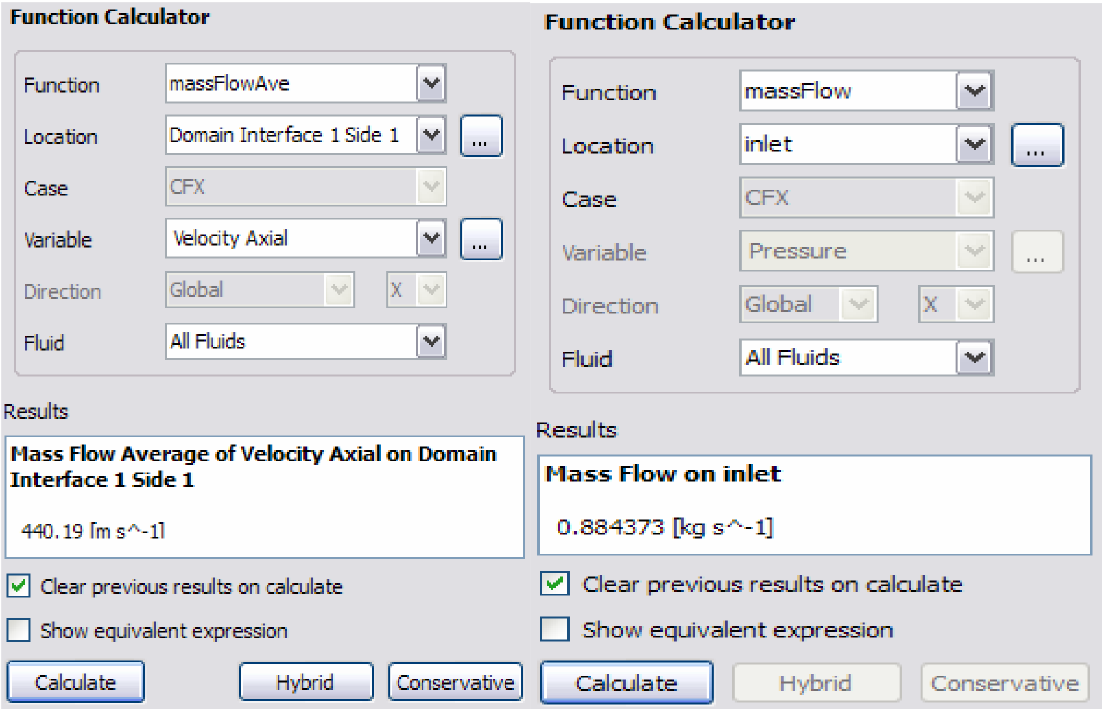

Fig. 24. – Obtained velocity and pressure values during the study

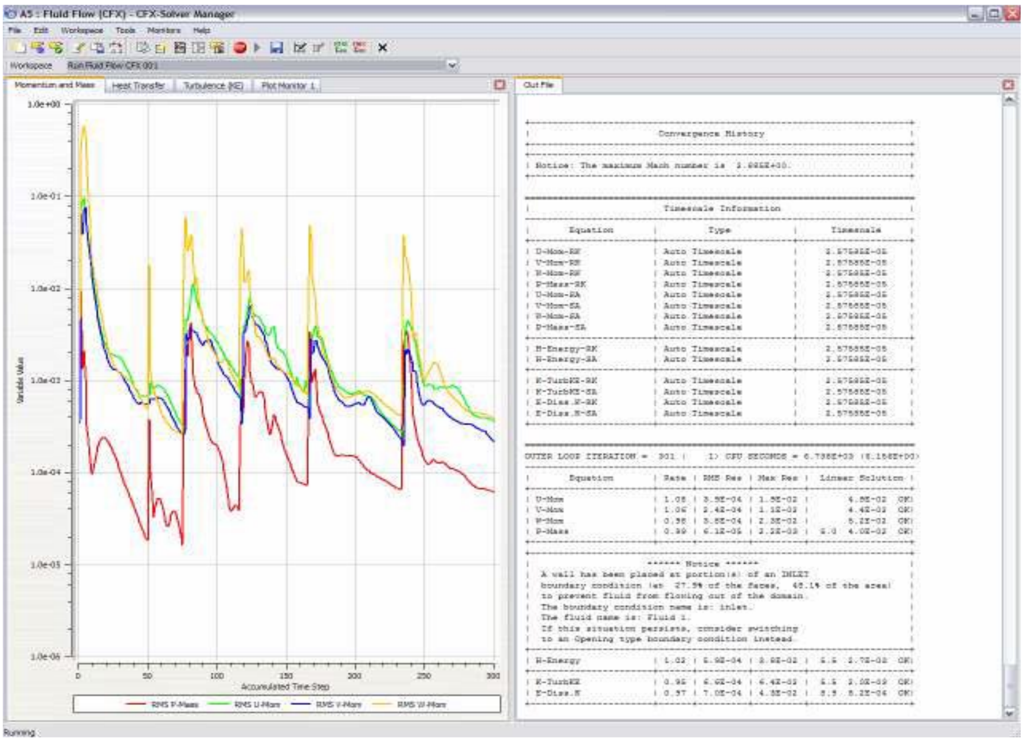

Fig. 25. - Analysis of the internal frequencies of the torque converter

Thus, it can be assumed that the manufacture of the impeller hub from parts, and the connection of these parts by welding and splined joints, was the cause of the development of all the above defects, since the resulting vibrations, as well as the presence of welds in the structure, and places for the development of defects, increase the risk explosive development of cracks and subsequent resolution or jamming of the entire assembly as a whole.

References

[1] Computer modeling of products and CAE-systems [Electronic resource] / Journal "CAD and graphics" - M., 2000. - Access mode: http://www.sapr.ru/Article.aspx?id=6668
[2] Rudakov K.N. Femap 10.2.0. Geometric and finite element modeling of structures. - K.: KPI, 2011. - 31 p.
[3] Technologies [Electronic resource] / "ALPLAST". - St. Petersburg, 2008. - Access mode: http:// www.alplast-spb.ru / technologies.htm.
[4] Filippovich, KV Ideology of post-processing in modern CAD/CAM systems / KV Filippovich // Russia: OOO Eurasia Limited, 2000 [Electronic resource]. - 2008. - Access mode: http:// www.sapr2000.ru / pressa2.html.
[5] Siemens PLM Software official site, NX6 system (Unigraphics) [Electronic resource]. - Access mode: www.plm.automation.siemens.com/ru_ru.
[6] Xiong Pan, Chen Xinyuan, Zhen Chenping Effect of internal leakage on torque converter characteristics //Advances in Mechanical Engineering, September 1, 2014, https://doi.org/10.1177/1687814020959969
[7] Shinya Kano,Yuji Terasaka, Kouzou Yano Prediction of Torque Converter Characteristics by Fluid Flow Simulation //Technical report, 2004, Vol. 50, No.154. – P.1 – 6.

Information of the authors

Nikonova Tatyana Yurievna, Candidate of Technical Sciences, Acting Associate Professor, Abylkas Saginov Karaganda Technical University
e-mail: nitka82@list.ru

Essyunin Alan Igorevich, Master student, Abylkas Saginov Karaganda Technical University
e-mail: alan_100299@mail.ru

Zhakupova Sholpan Serkenovna, Candidate of Philological Sciences, Abylkas Saginov Karaganda Technical University
e-mail: zhakshol@mail.ru

Dandybaev Esim Serikovich, Candidate of Technical Sciences, Senior Lecturer, Abylkas Saginov Karaganda Technical University
e-mail: esim.dandybayev@list.ru

Zhukova Alla Valentinovna, Senior Lecturer, Abylkas Saginov Karaganda Technical University
e-mail: aluny@mail.ru